Cyanobacterial formation of intracellular Ca-carbonates in undersaturated solutions

Nithavong Cam, Karim Benzerara, Thomas Georgelin, Maguy Jaber, Jean-François Lambert, Mélanie Poinsot, Fériel Skouri-Panet, David Moreira, Purificacion Lopez-Garcia, Emmanuelle Raimbault, et al.

Cyanobacterial formation of intracellular Ca-carbonates in undersaturated solutions

Running title: Cyanobacterial carbonatogenesis in undersaturated solutions

Nithavong Cam[1,2], Karim Benzerara[1], Thomas Georgelin[2], Maguy Jaber[3], Jean-François Lambert[2], Mélanie Poinsot[1], Fériel Skouri-Panet[1], David Moreira[4], Purificación López-García[4], Emmanuelle Raimbault[5], Laure Cordier[5], Didier Jézéquel[5]

[1]Institut de Minéralogie, de Physique des Matériaux, et de Cosmochimie (IMPMC), Sorbonne Universités, UPMC Univ Paris 6, UMR CNRS 7590, Muséum National d'Histoire Naturelle, IRD UMR 206, 4 Place Jussieu, 75005 Paris, France

[2]Laboratoire de Réactivité de Surface (LRS), Sorbonne Universités, UMR CNRS 7197, UPMC Univ Paris 6, 4 Place Jussieu, 75005 Paris, France

[3]Laboratoire d'Archéologie Moléculaire et Structurale (LAMS), Sorbonne Universités, UMR CNRS 8220, UPMC Univ Paris 6, 4 Place Jussieu, 75005 Paris, France

[4]Unité d'Ecologie, Systématique et Evolution, CNRS UMR 8079, Université Paris-Sud/Paris-Saclay, AgroParisTech, 91400 Orsay, France.

[5]Institut de Physique du Globe de Paris (IPGP), Sorbonne Paris Cité– Université Paris Diderot, UMR CNRS 7154, 1 rue Jussieu, 75238 Paris cedex 05, France

Corresponding author: Karim Benzerara, IMPMC, Case 115, 4 Place Jussieu 75005 Paris, France. Phone: 33144277542; Fax: 33144273785; karim.benzerara@upmc.fr

Conflict of interest. The authors declare no conflict of interest

Keywords: biomineralization; cyanobacteria; calcium homeostasis; polyphosphates

Abstract

Cyanobacteria have long been thought to induce the formation of Ca-carbonates as secondary byproducts of their metabolic activity, by shifting the chemical composition of their extracellular environment to conditions favoring mineral precipitation. Some cyanobacterial species forming Ca-carbonates intracellularly were recently discovered. However, the environmental conditions under which this intracellular biomineralization process can occur and the impact of cyanobacterial species forming Ca-carbonates intracellularly on extracellular carbonatogenesis are not known. Here, we show that these cyanobacteria can form Ca-carbonates intracellularly while growing in extracellular solutions undersaturated with respect to all Ca-carbonate phases, i.e., conditions thermodynamically unfavorable to mineral precipitation. This shows that intracellular Ca-carbonate biomineralization is an active process, i.e., it costs energy provided by the cells. The cost of energy may be due to the active accumulation of Ca intracellularly. Moreover, unlike cyanobacterial strains that have been usually considered before by studies on Ca-carbonate biomineralization, cyanobacteria forming intracellular carbonates may slow down or hamper extracellular carbonatogenesis, by decreasing the saturation index of their extracellular solution following the buffering of the concentration of extracellular calcium to low levels.

Introduction

Biomineralization of $CaCO_3$ by cyanobacteria has been thoroughly studied because of its consequences for the formation of ancient biogenic carbonate deposits and its impact on the global geochemical cycles of carbon and calcium (Riding, 2000; Jansson & Northen, 2010; Gérard *et al.*, 2013; Bundeleva *et al.*, 2014). $CaCO_3$ biomineralization by cyanobacteria is usually believed to result from their photosynthetic activity (Merz, 1992). More precisely,

cyanobacteria actively import inorganic carbon, mostly as HCO_3^- (Miller & Colman, 1980). Intracellular conversion of HCO_3^- to CO_2 by carbonic anhydrases followed by CO_2 fixation by Ribulose-1,5-bisphosphate carboxylase/oxygenase (RuBisCO) and the associated import of H^+ to regulate intracellular pH result in the increase of extracellular pH, which favors extracellular $CaCO_3$ precipitation (Verrecchia *et al.*, 1995; Badger & Price, 2003; Riding, 2006). The crucial role of carbonic anhydrases in carbonate biomineralization has been repeatedly noticed, not only for cyanobacteria but also for other calcifying organisms (e.g. in sponges, Jackson et al., 2007). At least in some cyanobacteria, Ca^{2+}/H^+ transmembrane exchangers regulate the intracellular concentration of Ca^{2+} at low levels by exporting Ca extracellularly, favoring further $CaCO_3$ biomineralization (Jiang *et al.*, 2013). Therefore, for many years, $CaCO_3$ biomineralization by cyanobacteria has been considered as exclusively extracellular and dependent on the chemical conditions prevailing in the extracellular environments of cyanobacterial cells. However, several species of cyanobacteria forming intracellular $CaCO_3$ granules were recently discovered (Couradeau *et al.*, 2012; Benzerara et al., 2014; Moreira *et al.*, 2017). Couradeau *et al.* (2012) tentatively suggested that these $CaCO_3$ granules may serve as ballasts increasing cell density and favoring a benthic mode of life. Alternatively, $CaCO_3$ granules may buffer intracellular pH. Finally, the formation of intracellular carbonates may have no biological function and may just be a byproduct of photosynthesis in cyanobacteria that do not regulate well intracellular pH and/or Ca^{2+} concentrations. Cyanobacteria forming intracellular $CaCO_3$ were found in various environments, including lakes, soils, karstic ponds and hydrothermal settings across the world (Benzerara *et al.*, 2014; Ragon *et al.*, 2014; Saghaï *et al.*, 2015). This suggests that diverse environmental conditions may allow intracellular calcification but these have yet to be explored further. Moreover, it raises the question of whether ancient cyanobacteria used to induce calcium carbonate precipitation intracellularly or extracellularly. This is important in order to figure out what fossil traces of these

75 microorganisms may be expected in the geological record (Riding, 2012). Indeed,
76 cyanobacteria favoring extracellular carbonatogenesis can get encrusted by the resulting
77 minerals under some conditions, forming calcimicrobes (e.g., Arp et al., 2001; Couradeau *et*
78 *al.*, 2013). In contrast, this may not be the case for cyanobacteria forming carbonates
79 intracellularly (Riding, 2012).
80 At least two different mechanisms of intracellular biomineralization may exist based on the
81 observation of two different distribution patterns of the intracellular $CaCO_3$ granules in cells
82 (Li *et al.*, 2016): 1) in one clade of cyanobacteria, $CaCO_3$ granules are mostly located at the
83 poles of the cells and nucleate at the division septum where cells divide. In this case, the
84 involvement of division proteins in the nucleation of ACC has been speculated. 2) In other
85 clades, $CaCO_3$ granules do not show this polar distribution and are scattered or form chains
86 within the cytoplasm (Li *et al.*, 2016). In all clades, granules are composed of amorphous
87 calcium carbonates (ACC) as determined by transmission electron microscopy selected area
88 electron diffraction (Benzerara et al., 2014). How these mineral phases with a relatively high
89 solubility form in the cytoplasm, supposedly undersaturated with ACC, remains enigmatic
90 (Cam *et al.*, 2015). It has been speculated that unlike cyanobacteria forming extracellular
91 carbonates, intracellularly calcifying cyanobacteria may decrease the saturation of the
92 extracellular solution with respect to $CaCO_3$ phases or at least not affect it at all (Couradeau *et*
93 *al.*, 2012). However, this assumption lacks experimental evidence. Moreover, it is not clear how
94 the different species of intracellularly calcifying cyanobacteria, especially those showing
95 different biomineralization patterns, may affect the supersaturation of their environment.
96 Here, we followed the changes with time of the chemical composition of the culture media of
97 three strains of cyanobacteria forming intracellular carbonates: *Gloeomargarita lithophora*
98 strain C7, *Thermosynechococcus elongatus* strain BP-1 and *Cyanothece sp.* strain PCC 7425
99 and one strain not forming intracellular carbonates: *Gloeocapsa* sp. strain PCC 73106. $CaCO_3$

granules are scattered within the cytoplasm in *G. lithophora* and *Cyanothece sp.* while they are located at cell poles in *T. elongatus*. We measured cell growth and chemical parameters such as concentrations of dissolved Ca^{2+} and HCO_3^- and pH to assess the saturation of the extracellular solution with various $CaCO_3$ phases. Moreover, we analyzed the intracellular distribution of Ca by electron microscopy analyses. This allows defining the environmental conditions necessary for intracellular calcification and how intracellularly calcifying cyanobacteria may affect their local environments.

MATERIALS AND METHODS

Cyanobacterial strains and culture conditions

Four cyanobacterial strains were cultured. Three strains encompassing most of the phylogenetic diversity of cyanobacteria that have been shown to form intracellular Ca-carbonates (Benzerara *et al.*, 2014) were studied: *Gloeomargarita lithophora* strain C7 enriched from an alkaline crater lake in Mexico as described by Moreira *et al.* (2017) and showing $CaCO_3$ granules scattered in the cytoplasm; the axenic strains *Cyanothece* sp. strain PCC 7425 isolated from a rice field in Senegal, described by (Rippka *et al.*, 1979) and (Porta *et al.*, 1999) and showing $CaCO_3$ granules scattered in the cytoplasm; the axenic strain *Thermosynechococcus elongatus* strain BP-1 isolated from a hot spring in Japan, described by Yamaoka *et al.* (1978) and Nakamura *et al.* (2002) and showing $CaCO_3$ granules at the poles. One strain not forming intracellular carbonates (Benzerara *et al.,* 2014) was used as a comparison for Ca uptake: the axenic strain *Gloeocapsa sp.* strain PCC 73106 isolated from a *Sphagnum* bog in Switzerland and described by (Rippka *et al.*, 1979). The choice of this strain as a control was motivated by the fact that *Gloeocapsa* was previously studied for its capabilities to induce extracellular carbonatogenesis (Bundeleva *et al.*, 2014) and *Gloeocapsa sp.* strain PCC 73106 can be cultured in the same medium as the three strains forming intracellular carbonates. It should be noted that

extracellular $CaCO_3$ precipitation by *Gloeocapsa sp.* was observed in solutions different from the BG11 medium used in the present study, in particular with much higher initial concentrations of dissolved Ca: 5-10 mM in Bundeleva et al. (2014) *vs*. 250 µM, here.

Strains were cultured in triplicates in medium BG-11 (Rippka *et al.*, 1979), under continuous light (5-10 $\mu mol.m^2.s^{-1}$) at 45 °C for *T. elongatus* and 30 °C for *G. lithophora, Cyanothece sp.* and *Gloeocapsa sp.* BG-11 is classically used to culture freshwater cyanobacterial strains. Its composition is available on http://cyanobacteria.web.pasteur.fr/. It mostly contains Na^+ and NO_3^- with ~180 µM of orthophosphates and ~250 µM of calcium. Evaporation was compensated by daily addition of sterile milli-Q water. The optical density (OD) of the cultures was measured at 730 nm to assess cell growth. The combined measurement of OD and cell counting on one sample allowed to derive the relationships between OD and cell density as 9×10^7, 3×10^7, 2.5×10^7 and 6.4×10^7 cells.mL^{-1}.OD $unit^{-1}$ for *G. lithophora*, *Cyanothece* sp., *T. elongatus* and *Gloeocapsa* sp., respectively. Similarly, the relationships between OD and cell dry mass were 3.6×10^{-4}, 2.4×10^{-4} and 3.2×10^{-4} g.mL^{-1}.OD $unit^{-1}$ for *G. lithophora*, *Cyanothece sp.* and *T. elongatus*, respectively.

Bulk chemical analyses of solutions

For chemical analyses, culture samples were centrifuged at 5,000 g for 10 min. The pH was measured in the supernatants. Variations of pH in non-inoculated sterile controls were less than 0.1. Supernatants were systematically filtered at 0.22 µm.

The concentration of dissolved calcium in filtered supernatants was measured by colorimetry based on the method described by (Moorehead & Biggs, 1974). Twenty-five microliters of filtered sample were added to 1 mL of a mix solution containing o-cresolphtalein complexone, hydrocholic acid, 8-hydroxyquinoline and 2-amino-2-methyl-1-propanol. The OD of the resulting solution was measured at 570 nm. Standard solutions of calcium at 1, 0.5, 0.25, 0.125,

0.1 and 0.05 mM were used for calibration. The detection limit for colorimetry measurements was 0.02 mM. Uptake rates normalized by the number of cells were determined for each time step as followed:

$$\frac{[Ca^{2+}]_{t-1} - [Ca^{2+}]_t}{average\ cell\ density\ between\ t_{-1}\ and\ t} / (t - t_{-1})$$

Where t and t_{-1} were consecutive sampling times, and the average density between t_{-1} and t was obtained as the arithmetic average of cell density derived from OD measurements. An alternative approach to measuring removal of dissolved Ca from the solution, would have been to measure Ca in the cells. This would involve an additional step of chemical extraction of Ca from the cells. We tested that these two approaches provide similar result (data not shown).

The total alkalinity is a form of mass-conservation relationship for hydrogen ion and is defined as: "the number of moles of hydrogen ion equivalent to the excess of proton acceptors (bases formed from weak acids with a dissociation constant $K \leq 10^{-4.5}$, at 25°C and zero ionic strength) over proton donors (acids with $K > 10^{-4.5}$) in one kilogram of sample" (Sarazin *et al.*, 1999). Here, alkalinity (Alk) was defined as:

$$Alk = [HCO_3^-] + 2[CO_3^{2-}] + [HPO_4^{2-}] + 2[PO_4^{3-}] + [NH_3] + [OH^-]$$

Alkalinity was measured by colorimetry. Five hundred microliters of filtered sample were added to 500 µL of a solution composed of formic acid at 3.5 mM and bromothymol blue at 30 $mg.L^{-1}$. The OD of the solution was measured at 590 nm and was related to the alkalinity by a second order relation (Sarazin *et al.*, 1999). The calibration was performed using standard $NaHCO_3$ solutions with concentrations between 0.5 and 3.5 mM with steps of 0.25.

Dissolved inorganic phosphorus (DIP) and ammonium (ΣNH_3) concentrations were measured by continuous flow colorimetry on a QuAAtro Axflow (Seal Analytical). Concentrations of dissolved chloride, sulfate, nitrite and nitrate were measured by ion-exchange chromatography using an ICS1100 Thermofisher on a Ionpac thermo AS14 column with an eluant composed of 3.5 mM of Na_2CO_3 and 1 mM of $NaHCO_3$ with a flow rate of 1.2 $mL.min^{-1}$. Nitrites and nitrates

were measured using a UVD340U detector. Concentrations of HCO_3^- were deduced from pH, alkalinity, dissolved phosphorus and ammonium measurements.

Concentrations of major dissolved cations, including Ca were measured using a Thermo Scientific™ iCAP™ 6200 inductively coupled plasma atomic emission spectrometer (ICP-AES) equipped with a Cetac ASX-520 autosampler. For ICP-AES analyzes, 300 µL of filtered supernatants were acidified with 10 mL of 2 % HNO_3. Measurements of Ca concentrations by ICP-AES and colorimetry were correlated along a 1:1 line with consistency better than 85 % (r^2 for the regression) above 50 µM.

Speciation and saturation indices calculations

The Visual MINTEQ (3.0) software (Gustafsson, 2013) with the Davies method (Davies *et al.*, 1962) was used to calculate the concentrations of species in the culture medium based on bulk chemical analyses. The cultures were supposed to be in free exchange with the atmosphere with a partial CO_2 pressure of 380 ppm following the procedure by (Siong and Asaeda, 2009). The saturation index was defined as:

$$SI = -\log [(CO_3^{2-})(Ca^{2+})/Ks]$$

Where () denotes the activity and Ks the solubility of a given phase. Saturation indices were calculated for all Ca-carbonate phases reported in the Visual MINTEQ database as well as for ACC using a Ks of 2.32×10^{-8} (Kellermeier *et al.*, 2014).

Scanning transmission electron microscopy (STEM) and energy dispersive x-ray spectrometry (EDXS) analyses

For microscopy analyses, cell pellets obtained by centrifugation were washed three times with milli-Q water before resuspension in 500 µL of milli-Q water and deposition of 3 µL on carbon-coated 200-mesh copper grids. Washing was necessary to avoid precipitation of salts upon drying. This sample preparation procedure was repeatedly used and tested in past studies on

cyanobacteria forming intracellular carbonates (Benzerara *et al.*, 2014; Li *et al.*, 2016). Although it may induce some alterations of the morphology of the cells (e.g., collapse), it allows the preservation of intracellular $CaCO_3$ inclusions on the contrary to procedures using chemical fixatives (Li *et al.*, 2016). The same procedure was also successfully used to study extracellular Ca-phosphate precipitates formed by bacterial cells (e.g., Cosmidis *et al.*, 2015). In the present study, only STEM analyses of $CaCO_3$ inclusions are discussed, not cell morphological features. STEM analyses were performed in the High Angle Annular Dark Field (HAADF) mode using a JEOL 2100F operating at 200 kV and equipped with a field emission gun, a high-resolution UHR pole piece, and a JEOL EDXS detector with an ultrathin window allowing detection of light elements. Semi-quantitative analyses of EDXS spectra was done using the JEOL Analysis Station software following the procedure by (Li *et al.*, 2016). This was based on the use of K-factors. After subtracting out the background noise in the EDXS spectrum, the software performed a Gaussian fit of selected elemental peaks and calculated the area under the peaks. From this, the atomic percentage of selected element was assessed: Ca, Mg in the carbonates; Ca, Mg, K and P in polyphosphates.

RESULTS

Cell growth and temporal changes of chemical parameters in growth medium

All strains grew in BG-11 at different rates (Fig. 1 and Fig. S1). During the exponential growth, generation times were 108 ± 2 h, 46 ± 1 h, 23 ± 2 h and 163 ± 19 h for *G. lithophora*, *Cyanothece* sp., *T. elongatus*, and *Gloeocapsa* sp., respectively (Fig. S1). In parallel, pH increased at different rates and reached different values for the different strains, starting from 7.5 up to 8.8, 9.2, 9.8 and 9.7 for *G. lithophora*, *Cyanothece* sp., *T. elongatus* and *Gloeocapsa* sp., respectively (Fig. 1). In contrast, the pH, optical density at 730 nm (OD) and

dissolved [Ca] remained constant over the duration of the experiment in a non-inoculated control BG-11 medium (Fig. S2).

The time evolution of dissolved extracellular Ca was significantly different for strains forming intracellular carbonates *vs. Gloeocapsa sp.*, which does not form intracellular Ca-carbonates. Calcium concentration decreased dramatically from ~250 µM down to 2.75 ± 0.54, 5.9 ± 1.3 and 12.8 ± 3.6 µM (n=3) for *G. lithophora*, *Cyanothece* sp. and *T. elongatus*, respectively (Table S1). For *G. lithophora* and *T. elongatus*, the decrease of Ca concentration varied in the opposite way to the OD and was linear with time at rates of 0.47 ± 0.06 and 0.79 ± 0.07 µM of Ca per hour. For *Cyanothece* sp., the decrease of Ca concentration also varied oppositely to OD but there was a short transient phase during which the concentration of dissolved Ca stopped decreasing and OD stopped increasing. This transient phase was not systematically observed in cultures of *Cyanothece sp*. Overall, when normalized to the number of cells, the Ca uptake rates varied in time and between strains from 0.07 to 0.01 $fmol.h^{-1}.cell^{-1}$, 0.11 to 0.001 $fmol.h^{-1}.cell^{-1}$ and 0.42 to 0.01 $fmol.h^{-1}.cell^{-1}$ for *G. lithophora*, *Cyanothece* sp. and *T. elongatus*, respectively (Fig. S3). In contrast to what was observed for strains forming intracellular carbonates, dissolved Ca concentration remained relatively constant for *Gloeocapsa sp.* cultures with only a slight decrease down to 183 µM.

The concentration of extracellular dissolved orthophosphates (here mostly HPO_4^{2-}) was measured in cultures where Ca concentration decreased significantly, i.e. cultures of strains forming intracellular Ca-carbonates, in order to test some potential correlation between these two parameters. There was some uptake of Ca and orthophosphates by the cells. Thereafter, what was incorporated by the cells is called the "fraction removed from the solution". From the measurements of dissolved Ca and orthophosphate at different times, it was possible to calculate the Ca/P of this fraction: it corresponds to the ratio between the amount of Ca and the amount of P removed from the solution between two consecutive time points (Fig. 2). Different

temporal evolutions were observed depending on the strains. For *G. lithophora*, the concentration of dissolved orthophosphates decreased with time but not in a constant ratio with Ca (Fig. 2). Indeed, the Ca/P ratio of the fraction removed from the solution decreased continuously from more than 2 down to around 0 when the concentration of dissolved Ca leveled down at 2.75 µM. For *Cyanothece* sp., there was only a slight decrease of dissolved orthophosphates from 170 down to 100 µM with a Ca/P of the fraction removed from the solution varying between 4 and 8 (Fig. 2). Finally, there was almost no variation of dissolved orthophosphates in *T. elongatus* cultures. Therefore, no correlation was observed overall between the temporal evolutions of dissolved Ca^{2+} and HPO_4^{2-} concentrations.

In all cultures, alkalinity (mostly $[HCO_3^-]$) increased continuously up to 3204, 4093 and 3591 µM for *G. lithophora*, *Cyanothece* sp. and *T. elongatus*, respectively (Fig. S4). This was due to the dissolution of atmospheric CO_2 which increased at increasing pH in BG11. Alkalinity was almost equal to $[HCO_3^-]$ in *G. lithophora* cultures. Some differences between alkalinity and $[HCO_3^-]$ (20 to 33 %, i.e., 0.8 to 1.2 mM) were observed in the late stages of the cultures of *Cyanothece* sp. and *T. elongatus*, due mostly to elevated concentrations of OH^- and CO_3^{2-} present in the solution (Fig. S4).

Moreover, Mg and S concentrations decreased while an increase of NO_2^- concentration was observed (Table S2-4). The measurement of all these concentrations allowed to calculate the speciation of elements in the extracellular solutions and their saturation indices (SI) with respect to different mineral phases, including Ca-carbonate and Ca-phosphate phases (Fig. 3; Table S5-7). For *G. lithophora*, the culture medium was constantly undersaturated with all Ca-carbonate phases, including ACC (Fig. 3). In contrast, the solution was supersaturated with hydroxyapatite at least until 650 h with SI values varying between 4.9 and 6.9 (Table S5). It became undersaturated with this phase after 650 h. For *Cyanothece* sp., solutions were always undersaturated with ACC and slightly supersaturated with calcite at two time points only (114

and 282 h; SI of around 1 and 0.2; Table S6). For *Thermosynechococcus elongatus*, solutions were slightly supersaturated with ACC at 162 and 234 h (SI of around 0.4 and 0.25, respectively; Table S7).

Intracellular distribution of Ca

The mass of incorporated Ca normalized to the total cell dry mass was estimated from bulk measurements for *G. lithophora*, *Cyanothece* sp. and *T. elongatus* cells (Fig. S5). Two processes impacted oppositely the time variation of this parameter: on the one hand, Ca uptake increased the normalized Ca mass content; on the other hand, cell division decreased it. The normalized mass of Ca at ~700 h amounted to 26 ± 3, 13 ± 2 and 15 ± 3 mg/g for *G. lithophora*, *Cyanothece* sp. and *T. elongatus*, respectively (Fig. S5). A slight decrease of the cellular mass proportion of Ca was observed for each strain after the time when extracellular dissolved Ca reached its minimum. This can be explained by the fact that cellular division was still continuing, while there was only little Ca left in the solutions. Standard deviations were too high to infer precisely the evolution of the cellular mass proportion of Ca in the first stages of growth.

In parallel, STEM observations were performed on cells pelleted at different stages of the culture (Fig. 4-6; Table S8-10). No extracellular Ca-containing precipitate was observed in the pellets. In contrast, most of *G. lithophora* (Fig. 4), *Cyanothece* sp. (Fig. 5) and *T. elongatus* cells (Fig. 6) contained intracellular granules with Ca. EDXS maps showed the presence of two different types of Ca-containing granules: 1) Ca-carbonates and 2) polyphosphates containing Mg and K and some Ca. Cells of the inoculum (t=0 h) appeared similar to cells observed by TEM at other stages and contained Ca-carbonates and polyphosphates as well (Table S8-10). *Gloeocapsa* sp. cells only contained polyphosphate granules with a little amount of Ca (Fig. S6).

Gloeomargarita lithophora cells contained a relatively constant number and volume of Ca-carbonates upon time, i.e., 7.8 ± 4.1 inclusions/cell and 0.058 ± 0.045 μm^3/cell, respectively (Table S8). Averages were calculated based on the number of observed cells, excluding cells which did not contain any intracellular granule. These cells with no intracellular granule represented 6 to 22 % of the total number of cells. The Mg/(Ca+Mg) ratio in the intracellular carbonates formed by *G. lithophora* was relatively constant between 9.8 and 14.8 % during most of the culture with one exception at 954 h when Mg/(Ca+Mg) ratios of 39 ± 18 % were measured. Considering the cellular mass proportion of Ca and a density of 2.18 $g.cm^{-3}$ for ACC (Fernandez-Martinez *et al.*, 2013), Ca contained in carbonate granules as observed by STEM represented between few percents and up to half of the total Ca bioaccumulated by *G. lithophora* cells. Since the measurements of cellular mass proportion of Ca by bulk analyses (ICP-AES) and STEM were independent and each was affected by relatively high uncertainties, the proportion of Ca contained by carbonates has to be considered as a very rough first order estimate.

Cyanothece sp. cells contained a relatively lower number of inclusions per cell (4.8 ± 2.8) but with larger diameters, representing a larger volume on average (Table S9). Between 8 and 36 % of the observed cells did not contain any inclusions in *Cyanothece sp.* cultures. Mg/(Ca+Mg) ratios of the carbonate granules were constant at around 4 %. Overall, Ca contained in carbonates represented between 16 and 76 % of total Ca in the cells.

Finally, *T. elongatus* cells contained a more variable number of inclusions, between 4 and 23, per cell (Table S10). The proportion of empty cells varied between 2 % and 21 %. Similarly to *Cyanothece sp.* cells, Mg/(Ca+Mg) ratios were constant at a low value (~4 %) except at 525 h, when they were slightly higher. Ca contained in carbonates represented a lower proportion (1.5-29 %) than what was estimated on average for *G. lithophora* and *Cyanothece sp.*

Overall, the different strains forming intracellular carbonates accumulated Ca with high affinity down to concentrations of few µM in the solutions, whatever their growth temperature and growth rate (Table S1). Moreover, it appears that the average number of $CaCO_3$ inclusions per cell and their diameter did not vary much with incubation time in a given strain. Therefore, it was not possible to infer the formation of $CaCO_3$ inclusions by observing single cells by TEM only (Table S8-10). However, with incubation time, there was an increasing number of cells with a constant number of inclusions per cell, i.e., an increasing total number of $CaCO_3$ inclusions in the cultures, attesting intracellular precipitation of ACC in cultures.

DISCUSSION

Changes of dissolved Ca concentrations are due to high cellular uptakes by intracellularly calcifying cyanobacteria

The concentration of dissolved Ca decreased significantly in the culture media of intracellularly calcifying cyanobacteria down to a few micromoles per liter. Several previous studies interpreted a similar decrease as the result of cellular uptake, although they sometimes used Ca concentrations of several millimolar, i.e., higher than in our study and therefore corresponding to a high supersaturation with respect to Ca-containing phases (Singh & Mishra, 2014). However, it has to be noticed that such a decrease of dissolved Ca concentrations may have two different origins: 1) extracellular precipitation of a Ca-rich phase and/or 2) uptake by the cells which includes sorption at their surface and accumulation within the cells. Here, culture media were supersaturated only with hydroxyapatite (SI= 0.9 to 10.1) at several time points for different strains. Therefore, Ca-phosphate precipitation may theoretically have occurred. However, several observations, when considered altogether, suggest that if Ca-phosphate

347 precipitation occurred, the decrease of dissolved Ca^{2+} was clearly not due to this process only
348 and cellular uptake and intracellular $CaCO_3$ precipitation were significant in all cases:

349 1) Sterile BG-11 was supersaturated with hydroxyapatite but no Ca decrease was observed
350 with time in non-inoculated controls. While this control is different in terms of pH and
351 the absence of possibly nucleating cell surfaces, it shows that supersaturation does not
352 imply effective precipitation.

353 2) Ca/P ratios of the fractions removed from the solutions were not constant over time, and
354 were very different between the cultures of different strains (Fig. 2). Therefore, the
355 fractions removed from the solution could not be a Ca-phosphate phase only, which
356 would have been characterized by a relatively constant Ca/P ratio. Moreover, Ca/P ratios
357 of the fractions removed from the solutions were most of the time not equal to the Ca/P
358 ratio of usual Ca-phosphates, which are comprised between 0.5 and 2 (Cosmidis *et al.*,
359 2015).

360 3) No extracellular Ca-phosphate precipitate was detected by STEM observations in all the
361 cultures.

362 4) Although extracellular solutions were supersaturated with hydroxyapatite at several
363 time points for *T. elongatus* cultures with a SI level up to 10.1 (the highest SI value
364 measured in all cultures), no significant decrease of dissolved P was observed. This
365 suggests that no significant precipitation of hydroxyapatite occurs at the SI values
366 measured in all these cultures. Under these conditions, despite the presence of cell
367 surfaces and high supersaturation, no Ca-phosphate precipitation occured.

368 5) For *G. lithophora* cultures, extracellular solutions became undersaturated with
369 hydroxyapatite and other Ca-phosphate phases after 450 h, indicating that Ca-
370 phosphates did not control the solubility of Ca in these cultures, hence the concentration
371 of extracellular dissolved Ca, in these experiments. Ca-phosphate phases may have in

turn precipitated within cells similarly to what was observed for amorphous $CaCO_3$ but such precipitates were not observed by TEM.

In contrast, the formation of polyphosphates, which were observed by STEM within cells of *Cyanothece sp.* and *G. lithophora* but very rarely in *T. elongatus* cells may better explain the observed decrease of dissolved P concentration in the cultures of *G. lithophora* and *Cyanothece sp.*

It is known that cyanobacterial surfaces sorb Ca^{2+}, at values of ~0.8 to 1.2 mg of calcium per g of dry matter for the cyanobacterium *Gloeocapsa* sp. (Bundeleva *et al.*, 2014) and this sometimes results in the precipitation of Ca-carbonates when extracellular solutions are supersaturated (Schultze-Lam *et al.*, 1992; Dittrich & Sibler, 2006; Obst *et al.*, 2009). It is also known that some Ca can also be complexed by intracellular proteins in bacteria (Gilabert, 2012; Domínguez *et al.*, 2015). Here, analyses by transmission electron microscopy on whole cells could not discriminate between these two pools of Ca. However, discriminating between these two pools is not crucial here since under the conditions used in the present study, most of the Ca was sequestered by polyphosphate and carbonate granules in cyanobacteria forming intracellular carbonates. This was shown by STEM analyses and the fact that amounts of Ca sorbed by *Gloeocapsa sp.* cells were small compared to total amounts of Ca accumulated by intracellularly calcifying strains. The mass of Ca in $CaCO_3$ inclusions was roughly assessed by TEM measurements, by counting the number of $CaCO_3$ inclusions per cell, measuring their volume, assessing their Mg/(Mg+Ca) ratios and taking into account the number of empty cells (Table S8-10). The comparison with the total Ca content in cells as measured by ICP-AES, suggested that Ca in $CaCO_3$ amounted 19-31 % in *G. lithophora*, 16-76 % in *Cyanothece sp.* and 1.5-29 % in *T. elongatus*. Considering all the uncertainties associated with these measurements and the difficulty to compare robustly TEM with ICP-AES measurements, we

consider that these numbers are consistent with the idea that ACC are important Ca reservoirs in these cells.

The three strains of cyanobacteria forming intracellular carbonates that were studied here accumulated calcium up to 20-40 mg per g of dry matter (2-4 % in mass). In comparison, *E. coli* cells accumulate a total of 0.19 mg of calcium per g of dry matter independently of the extracellular calcium concentration (Gangola and Rosen, 1987). Bundeleva *et al.* (2014) determined a maximum uptake of 0.8-1.2 mg of calcium per g of dry matter for the cyanobacterium *Gloeocapsa sp*. Spores of *Bacillus cereus* and *Bacillus megaterium*, which are notorious for being highly enriched in Ca, accumulate 14-23 mg/g of Ca (Foerster & Foster, 1966; Shibata *et al.*, 1992). Overall, this suggests that strains of intracellular carbonate-forming cyanobacteria tend to accumulate Ca to a larger extent than other strains, although this should be measured systematically for many other cyanobacterial strains. As a consequence, they also tend to buffer the extracellular dissolved calcium to a low concentration between 3 to 13 μM in batch cultures.

One implication of this high Ca uptake capability by cyanobacteria forming intracellular carbonates can be tentatively discussed. The high affinity of these cyanobacteria for Ca may decrease at least locally the concentration of dissolved Ca in the extracellular environment to low values, especially in cases when the local dissolved Ca pool is not replenished as fast as it is consumed by cells. In our batch experiments, where there is no replenishment of dissolved Ca, this decrease lowered saturation of the solutions with respect to Ca-containing phases, such as calcite or hydroxyapatite and therefore inhibited the precipitation of these mineral phases. In nature, if this uptake remains significant, even in supersaturated solutions, this may also inhibit or decrease the kinetics of $CaCO_3$ precipitation due to the lowering of the saturation index, at least locally around the cells. The formation of intracellular carbonates may therefore decrease the risk of cell encrustation by minerals, which is lethal in many cases (Couradeau *et al.*, 2013;

Miot *et al.*, 2015). Interestingly, different strategies have been developed by diverse microorganisms, all allowing to avoid cell encrustation. This is the case for 1) some iron-oxidizing bacteria, which induce a local decrease of pH (Hegler *et al.*, 2010) and/or produce templating extracellular polymers (Chan *et al.*, 2011) and 2) some cyanobacteria forming extracellular carbonates on a proteinaceous template (S layers) which can be shed from time to time (Schultze-Lam *et al.*, 1992). It is also interesting to note that such a lowering of solution saturation by active uptake of Ca inducing Ca-carbonate dissolution has been shown for some cyanobacterial euendoliths (Ramirez-Reinat and Garcia-Pichel, 2012).

Intracellular biomineralization is an active process: evidence and origin of the energy cost

Formation of intracellular ACC granules in the extracellular solutions undersaturated with Ca-carbonate suggests that at least locally around the granules, the intracellular solution was supersaturated with ACC, i.e., cellular activity maintained an intracellular chemical composition allowing precipitation of ACC and therefore different from that prevailing in the extracellular solution. Therefore, intracellular $CaCO_3$ biomineralization is an active process, i.e., it involves some energy cost to maintain a supersaturated environment in a globally undersaturated solution.

The origin of this energy cost can be discussed. Parameters controlling $CaCO_3$ precipitation are the activities of Ca^{2+} and CO_3^{2-}. The latter depends on the activity of HCO_3^- and pH. Many cyanobacteria actively import HCO_3^- using CO_2 concentrating mechanisms (CCM). This results in high intracellular HCO_3^- concentrations up to 30 mM as measured in *Synechococcus* sp. Nageli (strain RRIMP N1) and in *Chlorogloeopsis* sp. (strain ATCC 27193) (Badger & Andrews, 1982; Skleryk *et al.*, 1997). Active uptake of bicarbonates may therefore account, at least partly, for the energy cost necessary to intracellular $CaCO_3$ biomineralization. It would be interesting to measure the $\delta^{13}C$ composition of intracellular ACC in the future as a way to better

assess the potential source of C for these precipitates. However, while many cyanobacteria show CCM capabilities, many do not form intracellular ACC (Benzerara *et al.*, 2014). The specificity of cyanobacteria forming intracellular $CaCO_3$ may therefore rely on another process. The intracellular pH in cyanobacteria is regulated, between 6.8 and 7.9 based on measurements performed on strains *Arthrospira platensis* and *Synechocystis* sp. PCC 6803 (Belkin & Boussiba, 1991; Jiang *et al.*, 2013). This is however less than the extracellular pH measured here and therefore intracellular pH regulation does not favor intracellular $CaCO_3$ biomineralization. Only regulation of pH within vesicles at a value higher than in the extracellular solution may favor intracellular $CaCO_3$ granule biomineralization with a cost of energy. Finally, the intracellular concentration of free calcium has been shown to be regulated within cells at very low values, around 100-200 nM with some possible increase up to 2.6 µM in *Anabaena* sp. PCC 7120 (Torrecilla *et al.*, 2000; Barrán-Berdón *et al.*, 2011). This strain does not form intracellular $CaCO_3$ granules (Benzerara et al., 2014). The maintenance of a low Ca concentration also costs energy but does not favor $CaCO_3$ biomineralization. In contrast, in cyanobacteria forming intracellular $CaCO_3$, it is possible that the high Ca uptake that we observed accounts for some of the energy cost. The pH and/or inorganic carbon and Ca concentrations required for $CaCO_3$ precipitation can be calculated, considering the approximation that the volume in which biomineralization occurs is filled with water containing Ca^{2+} and inorganic carbon only. At a Ca^{2+} concentration of 2.6 µM (i.e., maximum intracellular Ca concentration reported in the literature), this solution would be undersaturated with ACC even at a pH of 13 and 450 mM of inorganic carbon (SI=-1). Therefore, Ca^{2+} concentration is most likely higher at least locally where $CaCO_3$ granules form. The pH of the solution where ACC forms, possibly within submicrometer-scale compartments, might be locally high. This will be important to determine whether such intracellular pH heterogeneities exist in future studies despite the challenge of measuring such local variations in cells. Considering a pH of

7.9, and an inorganic carbon concentration of 30 mM, which are the maxima reported in the literature for the cytoplasm of cyanobacteria, the solution would be saturated with ACC for a Ca^{2+} concentration higher than 441 µM, i.e., higher than the initial Ca concentration in BG-11 and much higher than the extracellular dissolved Ca concentrations down to which *G. lithophora* ($[Ca]_{min}$=2.75 µM ± 0.54), *T. elongatus* ($[Ca]_{min}$=12.8 µM ± 3.6) and *Cyanothece sp.* ($[Ca]_{min}$=5.9 µM ± 1.3) accumulate Ca. Even if intracellular solutions are not pure water and solubility of ACC might be modified by the presence of organics (Giuffre *et al.*, 2013), this suggests that some active concentration of Ca may operate in intracellularly calcifying cyanobacteria involving some energy cost. Accordingly, cyanobacteria forming intracellular carbonates seem to accumulate Ca up to high levels as discussed above. This may appear surprising considering that such high cytoplasmic concentrations of Ca have been suggested to be toxic (e.g., Verhratsky and Parpura, 2014). It will be useful that future studies manage to measure intracellular free Ca^{2+} in cyanobacteria forming intracellular $CaCO_3$ and compare these concentrations with those measured in cyanobacteria not forming intracellular $CaCO_3$. However, one possibility is that intracellularly calcifying cyanobacteria regulate the cytoplasmic concentration of Ca at a low value around 100-200 nM as observed in all other bacteria and form intracellular compartments with a higher Ca concentration, in which Ca-carbonates precipitate (Fig. 7). This would require an active import of Ca from the cytosol to this compartment. The measured Ca uptake rates per cell, which vary with culture age and between species from 0.001 up to 0.42 $fmol.h^{-1}.cell^{-1}$, may depend on the physiological state of the cells as well as the efficiency of the transport systems of the different species. Despite relatively large error bars, uptake rates normalized by cell numbers and measured in the present study under these specific conditions will be interesting to compare with rates measured under varying conditions and other strains in future studies. The presence of a compartment would also mean that intracellular $CaCO_3$ formation by cyanobacteria is a controlled biomineralization

process involving specific cellular structures. Recent attempts to prepare ultramicrotomy thin sections for TEM investigations, preserving ACC granules have been unsuccessful (Li et al., 2016). Therefore, the existence of membranes delimitating potential compartments enclosing ACC granules remains speculative. Future cryo-microscopy observations may help to test further that hypothesis (Li *et al.*, 2016). The selective advantage provided by such an active accumulation of Ca will also need clarification in the future, whether it may serve as a Ca-detoxification or a storage mechanism. Based on the recognition that high Ca^{2+} concentrations can be toxic (Degens and Ittekkot, 1986) and the observation of intracellular Ca-containing amorphous granules in a phylogenetically broad range of animals (Simkiss, 1977), it has been previously suggested that Ca-detoxification is a widespread process. Whatever the origin of the energy cost for intracellular $CaCO_3$ biomineralization, the present observations have another implication regarding the preservation of fossil traces of this biomineralization capability. Once cells die, if the intracellular and extracellular solutions equilibrate and if the extracellular solution is undersaturated with ACC, ACC granules may dissolve and therefore may not be easily preserved as fossils. This might also explain the observation of cells with no ACC granules here (up to 36 % in *Cyanothece* sp. cultures after 623 h), which may be dead or inactive but this will require further analyses to determine the number of live/dead cells. In contrast, how these ACC granules may possibly transform to crystalline granules or may remain preserved in dead cells when the extracellular solution is supersaturated will be an interesting issue to investigate in order to better assess the fossilization potential of these cyanobacteria in the geological record.

Acknowledgments

Nithavong Cam salary was supported by French state funds managed by the ANR within the Investissements d'Avenir programme under reference ANR-11-IDEX-0004-02, and more specifically within the framework of the Cluster of Excellence MATISSE. Karim Benzerara has been supported by funding from the European Research Council under the European Community's Seventh Framework Programme (FP7/2007-2013 Grant Agreement no.307110 - ERC CALCYAN). The TEM facility at IMPMC was purchased owing to a support by Region Ile-de-France grant SESAME 2000 E 1435.

Supplementary information is available at (journal name)'s website

References

1. Arp G, Reimer A, Reitner J (2001) Photosynthesis-induced biofilm calcification and calcium concentrations in Phanerozoic oceans. *Science* **292**, 1701-1704.
2. Badger MR, Andrews TJ (1982) Photosynthesis and Inorganic Carbon Usage by the Marine Cyanobacterium, *Synechococcus sp. Plant Physiology* **70**, 517–523.
3. Badger MR, Price GD (2003) CO_2 concentrating mechanisms in cyanobacteria: molecular components, their diversity and evolution. *Journal of Experimental Botany* **54**, 609–622.
4. Barrán-Berdón AL, Rodea-Palomares I, Leganés, F, Fernández-Piñas F (2011) Free Ca^{2+} as an early intracellular biomarker of exposure of cyanobacteria to environmental pollution. *Analytical and Bioanalytical Chemistry* **400**, 1015–1029.
5. Belkin S, Boussiba S (1991) High internal pH conveys ammonia resistance in *Spirulina platensis*. *Bioresource Technology* **38**, 167–169.

543 6. Benzerara K, Skouri-Panet, F, Li J, Férard, C, Gugger M, Laurent T, et al. (2014)
544 Intracellular Ca-carbonate biomineralization is widespread in cyanobacteria.
545 *Proceedings of the National Academy of Sciences of the USA* **111**, 10933–10938.
546 7. Bundeleva IA, Shirokova LS, Pokrovsky OS, Bénézeth P, Ménez B, Gérard E, et al.
547 (2014) Experimental modeling of calcium carbonate precipitation by cyanobacterium
548 *Gloeocapsa sp*. *Chemical Geology* **374–375**, 44–60.
549 8. Cam N, Georgelin T, Jaber M, Lambert J-F, Benzerara K (2015) In vitro synthesis of
550 amorphous Mg-, Ca-, Sr- and Ba-carbonates: What do we learn about intracellular
551 calcification by cyanobacteria? *Geochimica Cosmochimica Acta* **161**, 36–49.
552 9. Chan CS, Fakra SC, Emerson D, Fleming EJ, Edwards KJ (2011) Lithotrophic iron-
553 oxidizing bacteria produce organic stalks to control mineral growth: implications for
554 biosignature formation. *ISME Journal* **5**, 717–727.
555 10. Cosmidis J, Benzerara K, Guyot F, Skouri-Panet F, Duprat E, Férard C, et al. (2015)
556 Calcium-phosphate biomineralization induced by alkaline phosphatase activity in
557 *Escherichia coli*: localization, kinetics, and potential signatures in the fossil record.
558 *Frontiers in Earth Science* **3**, article 84.
559 11. Couradeau E, Benzerara K, Gérard E, Estève I, Moreira D, Tavera R et al. (2013)
560 Cyanobacterial calcification in modern microbialites at the submicrometer scale.
561 *Biogeosciences* **10**, 5255–5266.
562 12. Couradeau E, Benzerara K, Gerard E, Moreira D, Bernard S, Brown GE et al. (2012)
563 An early-branching microbialite cyanobacterium forms intracellular carbonates.
564 *Science 336*, 459–462.
565 13. Davies CW (1962) Ion Association. Butterworths London.
566 14. Degens ET, Ittekkot V (1986) Ca^{2+}-stress, biological response and particle aggregation
567 in the aquatic habitat. *Netherlands Journal of Sea Research* 20, 109-116.

15. Dittrich M, Sibler S (2006) Influence of H^+ and Calcium Ions on Surface Functional Groups of *Synechococcus* PCC 7942 Cells. *Langmuir* **22**, 5435–5442.
16. Domínguez DC, Guragain M, Patrauchan M (2015) Calcium binding proteins and calcium signaling in prokaryotes. *Cell Calcium* **57**, 151–165.
17. Fernandez-Martinez A, Kalkan B, Clark SM, Waychunas GA (2013) Pressure-induced polyamorphism and formation of "aragonitic" amorphous calcium carbonate. *Angewandte Chemie International Edition* **52**, 8354–8357.
18. Foerster HF, Foster JW (1966) Endotrophic calcium, strontium, and barium spores of *Bacillus megaterium* and *Bacillus cereus*. *Journal of Bacteriology* **91**, 1333–1345.
19. Gangola P, Rosen BP (1987) Maintenance of intracellular calcium in *Escherichia coli*. *Journal of Biological Chemistry* **262**, 12570–12574.
20. Gérard E, Ménez B, Couradeau E, Moreira D, Benzerara K, Tavera R et al. (2013) Specific carbonate–microbe interactions in the modern microbialites of Lake Alchichica (Mexico). *ISME Journal* **7**, 1997–2009.
21. Gilabert JA (2012) Cytoplasmic calcium buffering In *Calcium Signaling* (ed Islam MS). Springer Science & Business Media, Dordrecht, pp. 483-498.
22. Giuffre AJ, Hamm LM, Han N, Yoreo JJD, Dove PM (2013) Polysaccharide chemistry regulates kinetics of calcite nucleation through competition of interfacial energies. *Proceedings of the National Academy of Sciences of the USA* **110**, 9261–9266.
23. Gustafsson JP (2013) Visual MINTEQ version 3.1, http://vminteq.lwr.kth.se/
24. Hegler F, Schmidt C, Schwarz H, Kappler A (2010) Does a low-pH microenvironment around phototrophic FeII-oxidizing bacteria prevent cell encrustation by FeIII minerals? *FEMS Microbiology Ecology* **74**, 592–600.
25. Jackson DJ, Macis L, Reitner J, Degnan BM, Worheide G (2007) Sponge paleogenomics reveals an ancient role for carbonic anhydrase in skeletogenesis. *Science* **316**, 1893-1895.

26. Jansson C, Northen T (2010) Calcifying cyanobacteria—the potential of biomineralization for carbon capture and storage. *Current Opinion in Biotechnology* **21**, 365–371.

27. Jiang H-B, Cheng H-M, Gao K-S, Qiu B-S (2013) Inactivation of Ca^{2+}/H^{+} Exchanger in *Synechocystis sp.* Strain PCC 6803 promotes cyanobacterial calcification by upregulating CO_2-concentrating mechanisms. *Applied and Environmental Microbiology* **79**, 4048–4055.

28. Kellermeier M, Picker A, Kempter A, Cölfen H, Gebauer D (2014) A straightforward treatment of activity in aqueous $CaCO_3$ solutions and the consequences for nucleation Theory. *Advanced Materials* **26**, 752–757.

29. Li J, Margaret Oliver I, Cam N, Boudier T, Blondeau M, Leroy E, et al. (2016) biomineralization patterns of intracellular carbonatogenesis in cyanobacteria: molecular hypotheses. *Minerals* **6**, 10.

30. Merz MU (1992) The biology of carbonate precipitation by cyanobacteria. *Facies* **26**, 81–101.

31. Miller AG, Colman B (1980) Evidence for HCO_3^- transport by the blue-green alga (Cyanobacterium) *Coccochloris peniocystis*. *Plant Physiology* **65**, 397–402.

32. Miot J, Remusat L, Duprat E, Gonzalez A, Pont S, Poinsot M (2015) Fe biomineralization mirrors individual metabolic activity in a nitrate-dependent Fe(II)-oxidizer. *Frontiers in Microbiology* **6**,

33. Moorehead WR, Biggs HG (1974) 2-Amino-2-methyl-1-propanol as the alkalizing agent in an improved continuous-flow cresolphthalein complexone procedure for calcium in serum. *Clinical Chemistry* **20**, 1458–1460.

34. Moreira D, Tavera R, Benzerara K, Skouri-Panet F, Couradeau E, Gérard E, Loussert Fonta C, Novelo E, Zivanovic Y, López-García P (2017) Description of

619 *Gloeomargarita lithophora* gen. nov., sp. nov., a thylakoid-bearing basal branching
620 cyanobacterium with intracellular carbonates, and proposal for Gloeomargaritales ord.
621 nov. *International Journal of Systematic and Evolutionary Microbiology*, in press
622 35. Nakamura Y, Kaneko T, Sato S, Ikeuchi M, Katoh H, Sasamoto S, et al. (2002)
623 Complete genome structure of the thermophilic cyanobacterium *Thermosynechococcus*
624 *elongatus* BP-1. *DNA Research* **9**, 123–130.
625 36. Obst M, Wehrli B, Dittrich M (2009) $CaCO_3$ nucleation by cyanobacteria: laboratory
626 evidence for a passive, surface-induced mechanism. *Geobiology* **7**, 324–347.
627 37. Porta D, Rippka R, Hernández-Mariné M (1999) Unusual ultrastructural features in
628 three strains of Cyanothece (cyanobacteria). *Archives in Microbiology* **173**, 154–163.
629 38. Ragon M, Benzerara K, Moreira D, Tavera R, López-García P (2014) 16S rDNA-based
630 analysis reveals cosmopolitan occurrence but limited diversity of two cyanobacterial
631 lineages with contrasted patterns of intracellular carbonate mineralization. *Frontiers in*
632 *Microbiology* **5**, 331.
633 39. Ramírez-Reinat EL and Garcia-Pichel F (2012) Prevalence of Ca^{2+}-ATPase-mediated
634 carbonate dissolution among cyanobacterial euendoliths. *Applied and Environmental*
635 *Microbiology* **78**, 7-13.
636 40. Riding R (2006) Cyanobacterial calcification, carbon dioxide concentrating
637 mechanisms, and Proterozoic/Cambrian changes in atmospheric composition.
638 *Geobiology* **4**, 299–316.
639 41. Riding R (2000) Microbial carbonates: the geological record of calcified bacterial–algal
640 mats and biofilms. *Sedimentology* **47**, 179–214.
641 42. Riding R (2012) A hard life for cyanobacteria. *Science* **336**, 427-428.

642 43. Rippka R, Deruelles J, Waterbury JB, Herdman M, Stanier RY (1979) Generic
643 assignments, strain histories and properties of pure cultures of Cyanobacteria. *Journal*
644 *of General Microbiology* **111**, 1–61.
645 44. Saghaï A, Zivanovic Y, Zeyen N, Moreira D, Benzerara K, Deschamps P, et al. (2015)
646 Metagenome-based diversity analyses suggest a significant contribution of non-
647 cyanobacterial lineages to carbonate precipitation in modern microbialites. *Frontiers in*
648 *Microbiology* **6**, 797.
649 45. Sarazin G, Michard G, Prevot F (1999) A rapid and accurate spectroscopic method for
650 alkalinity measurements in sea water samples. *Water Research* **33**, 290–294.
651 46. Schultze-Lam S, Harauz G, Beveridge TJ (1992) Participation of a cyanobacterial S
652 layer in fine-grain mineral formation. *Journal of Bacteriology* **174**, 7971–7981.
653 47. Shibata H, Miyoshi S, Osato T, Tani I, Hashimoto T (1992) Involvement of calcium in
654 germination of coat-modified spores of *Bacillus cereus* T. *Microbiology and*
655 *Immunology* **36**, 935–946.
656 48. Simkiss K (1977) Biomineralization and detoxification. *Calcified Tissue Research* **24,**
657 199.
658 49. Singh S, Mishra AK (2014) Regulation of calcium ion and its effect on growth and
659 developmental behavior in wild type and ntcA mutant of *Anabaena sp.* PCC 7120 under
660 varied levels of $CaCl_2$. *Microbiology* **83**, 235–246.
661 50. Siong K, Asaeda T (2009) Calcite encrustation in macro-algae *Chara* and its implication
662 to the formation of carbonate-bound cadmium. *Journal of Hazardous Materials* **167**,
663 1237–1241.
664 51. Skleryk RS, Tyrrell PN, Espie GS (1997) Photosynthesis and inorganic carbon
665 acquisition in the cyanobacterium *Chlorogloeopsis sp.* ATCC 27193. *Physiologia*
666 *Plantarum* **99**, 81–88.

52. Torrecilla I, Leganés F, Bonilla I, Fernández-Piñas F (2000) Use of recombinant aequorin to study calcium homeostasis and monitor calcium transients in response to heat and cold shock in cyanobacteria. *Plant Physiology* **123**, 161–176.

53. Verkhratsky A, Parpura V (2014) Calcium signaling and calcium channels: Evolution and general principles. *European Journal of Pharmacology* **739**, 1-3.

54. Verrecchia EP, Freytet P, Verrecchia KE, Dumont J-L (1995) Spherulites in calcrete laminar crusts: biogenic $CaCO_3$ precipitation as a major contributor to crust formation. *Journal of Sedimentary Research* **65A**, 690–700.

55. Yamaoka T, Satoh K, Katoh S (1978) Photosynthetic activities of a thermophilic blue-green alga. *Plant Cell Physiol*ogy **19**, 943–954.

679

680 **Figure legends**

681 **Fig. 1.** Time evolution of pH (open squares), optical density at 730 nm (closed circles) and
682 dissolved Ca (closed triangles). The pH and OD were measured in cultures of *G. lithophora*
683 (A), *Cyanothece* sp. (B), *Thermosynechococcus elongatus* (C) and *Gloeocapsa* sp. (D).
684 Dissolved Ca concentrations are shown separately for cultures of *G. lithophora* (E), *Cyanothece*
685 sp. (F), *Thermosynechococcus elongatus* (G) and *Gloeocapsa* sp. (H). Error bars were
686 calculated based on variations in triplicates and the precision of calcium concentration
687 measurements.

688

689 **Fig. 2.** Time evolution of the concentration of DIP ($[HPO_4^{2-}]$) and the Ca/P ratio of the fraction
690 incorporated by the cells. A, B and C correspond to DIP in cultures of *Gloeomargarita*
691 *lithophora* (A), *Cyanothece* sp. (B) and *Thermosynechococcus elongatus* (C). For all three
692 strains, error bars were calculated based on variations in triplicate cultures. When not visible,
693 error bars are smaller than the size of the symbols. Ca/P ratios of the fraction incorporated by
694 the cells are shown separately for cultures of *Gloeomargarita lithophora* (D), *Cyanothece* sp.
695 (E) and *Thermosynechococcus elongatus* (F). For these graphs, the three replicates are
696 represented by the different symbols (circle for replicate 1, triangle for replicate 2 and square
697 for replicate 3).

698

699 **Fig. 3.** Time evolution of the saturation index (SI) of solutions with calcite (filled circles) and
700 amorphous calcium carbonate (filled triangles) in cultures of *Gloeomargarita lithophora* (A),
701 *Cyanothece* sp. (B) and *Thermosynechococcus elongatus* (C). Error bars were calculated based
702 on variations in triplicates.

703

Fig. 4. STEM-EDXS analyses of *Gloeomargarita lithophora* cells collected after 186 h (A, B and C), and 645 h (D, E and F). (A and D) STEM-HAADF images showing bright carbonates (red circles) and light grey polyphosphate (green circles) granules. (B and E) Corresponding EDXS maps of carbon (blue), phosphorus (green) and calcium (red). (C and F) EDXS spectra of P-granules (green) and the Ca-granules (red) shown in A and D. Time points at which cells were collected are reported on the growth curve.

Fig. 5. STEM-EDXS analyses of *Cyanothece sp*. cells collected after 114 h (A, B and C) and 624 h (D, E and F) of culture. (A and D) STEM-HAADF images showing bright carbonates (red circles) and light grey polyphosphate (green circles) granules. (B and E) Corresponding EDXS maps of carbon (blue), phosphorus (green) and calcium (red). (C and F) EDXS spectra of P-granules (green), Ca-granules (red) and cell zone without granules shown in A and D. Time points at which cells were collected are reported on the growth curve.

Fig. 6. STEM-EDXS analyses of *Thermosynechococcus elongatus* cells collected after 162 h (A, C, D and E) and 525 h (B, F, G and H) of culture. (A, B, C and F) STEM-HAADF images showing bright carbonates (red circles) and light grey polyphosphate (green circles) granules. (D and G) Corresponding EDXS maps of carbon (blue), phosphorus (green) and calcium (red). (E and H) EDXS spectra of P-granules (green) and Ca-granules (red) shown in C and F. Time points at which cells were collected are reported on the growth curve.

Fig. 7. Scheme showing one hypothesis for the formation of intracellular carbonate inclusions. In this scenario, calcium exchanges between the cytoplasm and the extracellular medium follow the classical scheme as described in the literature, i.e., calcium is passively transported inwards and actively exported outwards. Moreover, Ca is actively transported from the cytoplasm to a

729 putative intracellular compartment where Ca-carbonate granules form. The thin and thick
730 arrows correspond to passive and active transport of calcium, respectively.
731
732
733

Figure 1

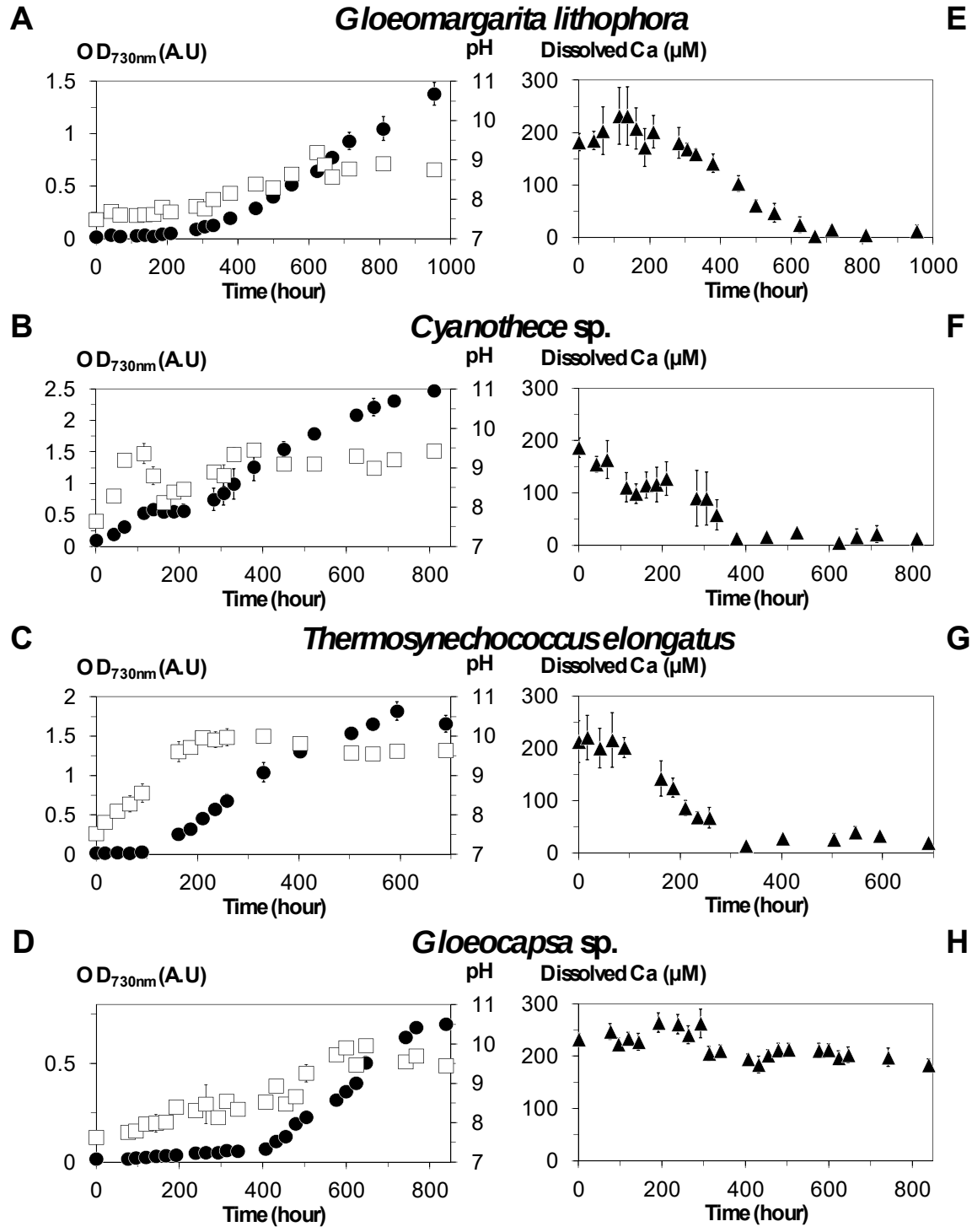
A
Gloeomargarita lithophora
E
OD730nm (A.U)
pH
Dissolved Ca (µM)
Time (hour)
B
Cyanothece sp.
F
C
Thermosynechococcus elongatus
G
D
Gloeocapsa sp.
H

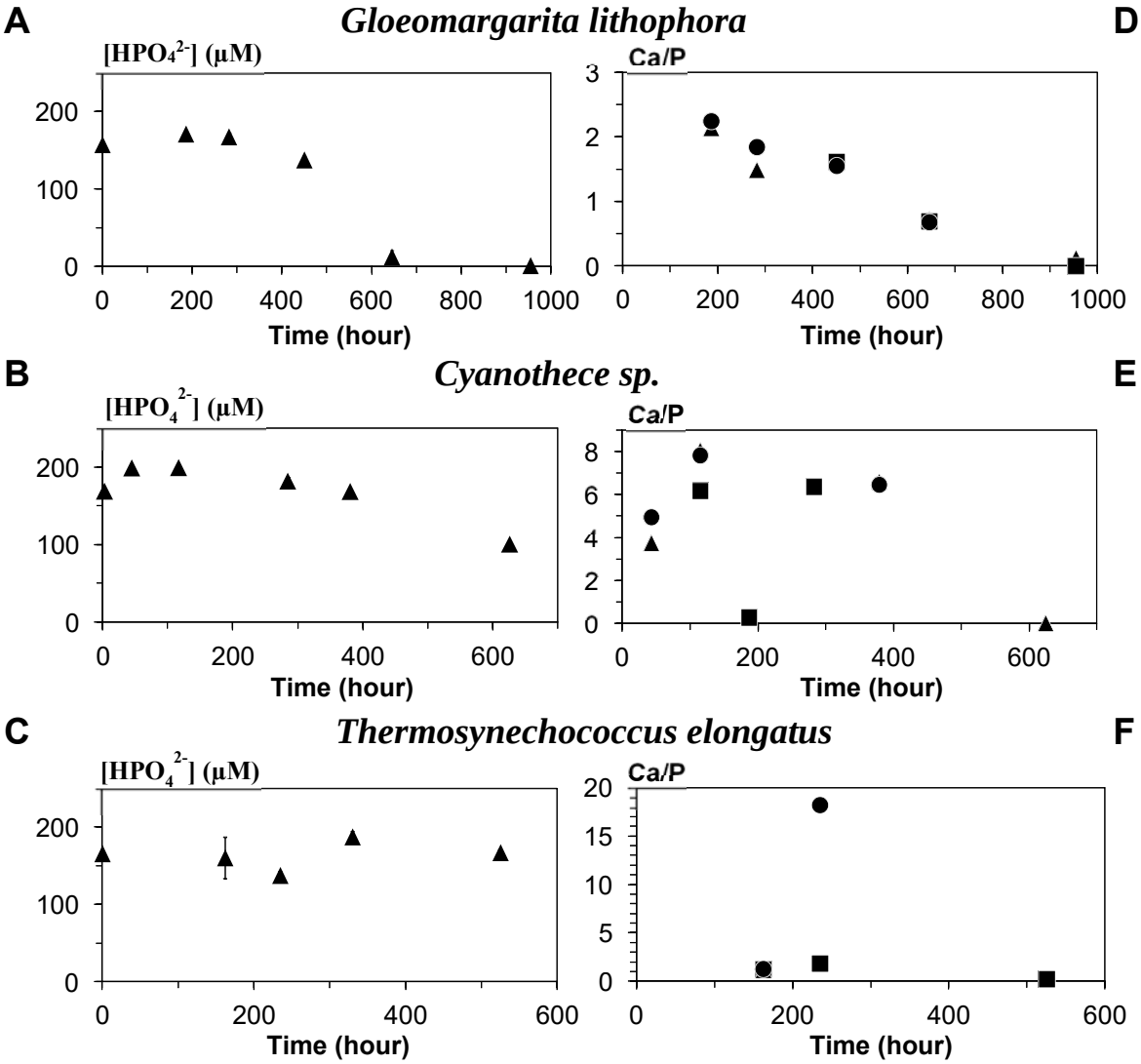
A
Gloeomargarita lithophora
D
[HPO4 2-] (µM)
Ca/P
Time (hour)
B
Cyanothece sp.
E
C
Thermosynechococcus elongatus
F

Figure 3

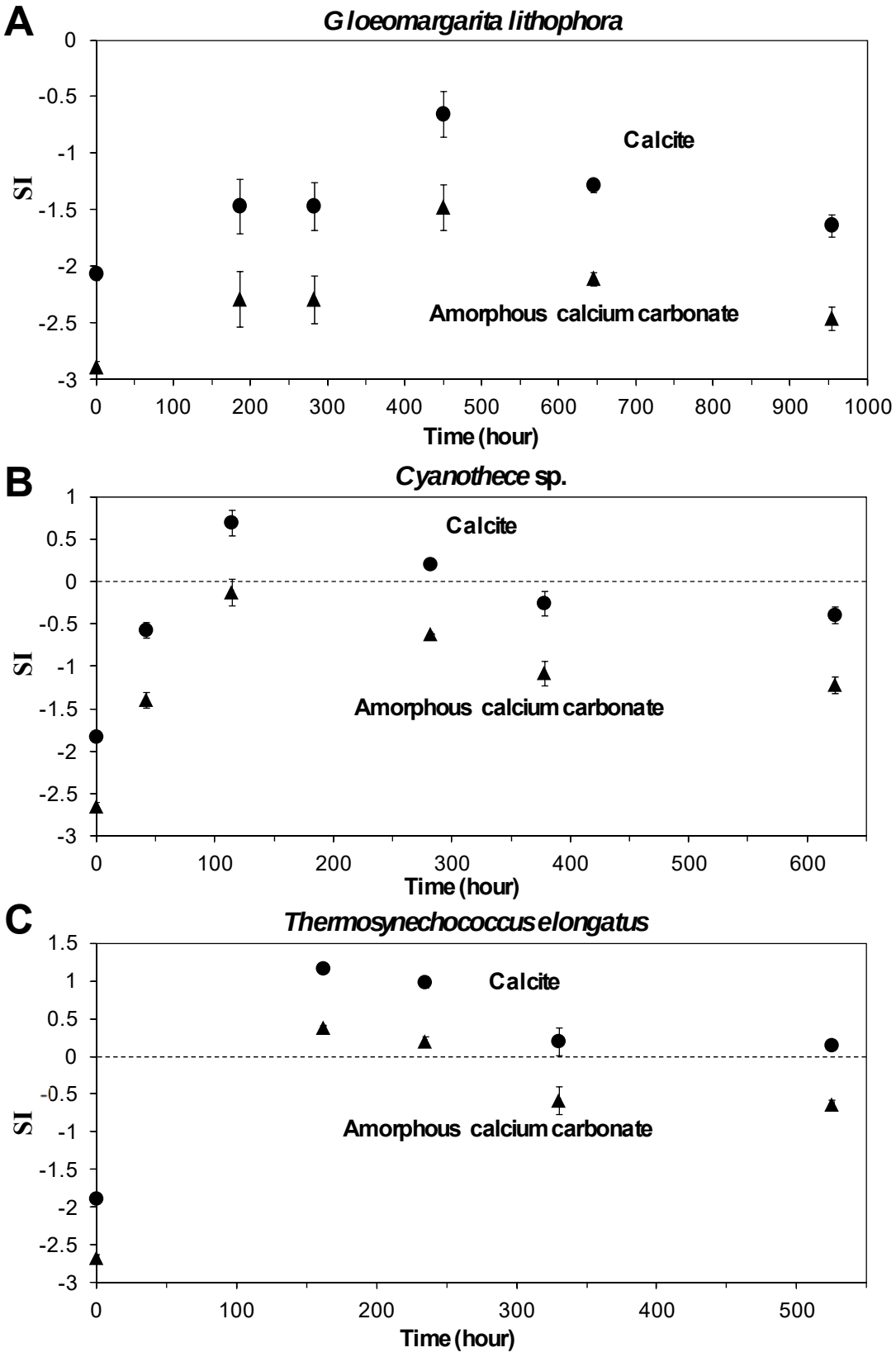
A
Gloeomargarita lithophora
SI
Calcite
Amorphous calcium carbonate
Time (hour)
B
Cyanothece sp.
SI
Calcite
Amorphous calcium carbonate
Time (hour)
C
Thermosynechococcus elongatus
SI
Calcite
Amorphous calcium carbonate
Time (hour)

Figure 4

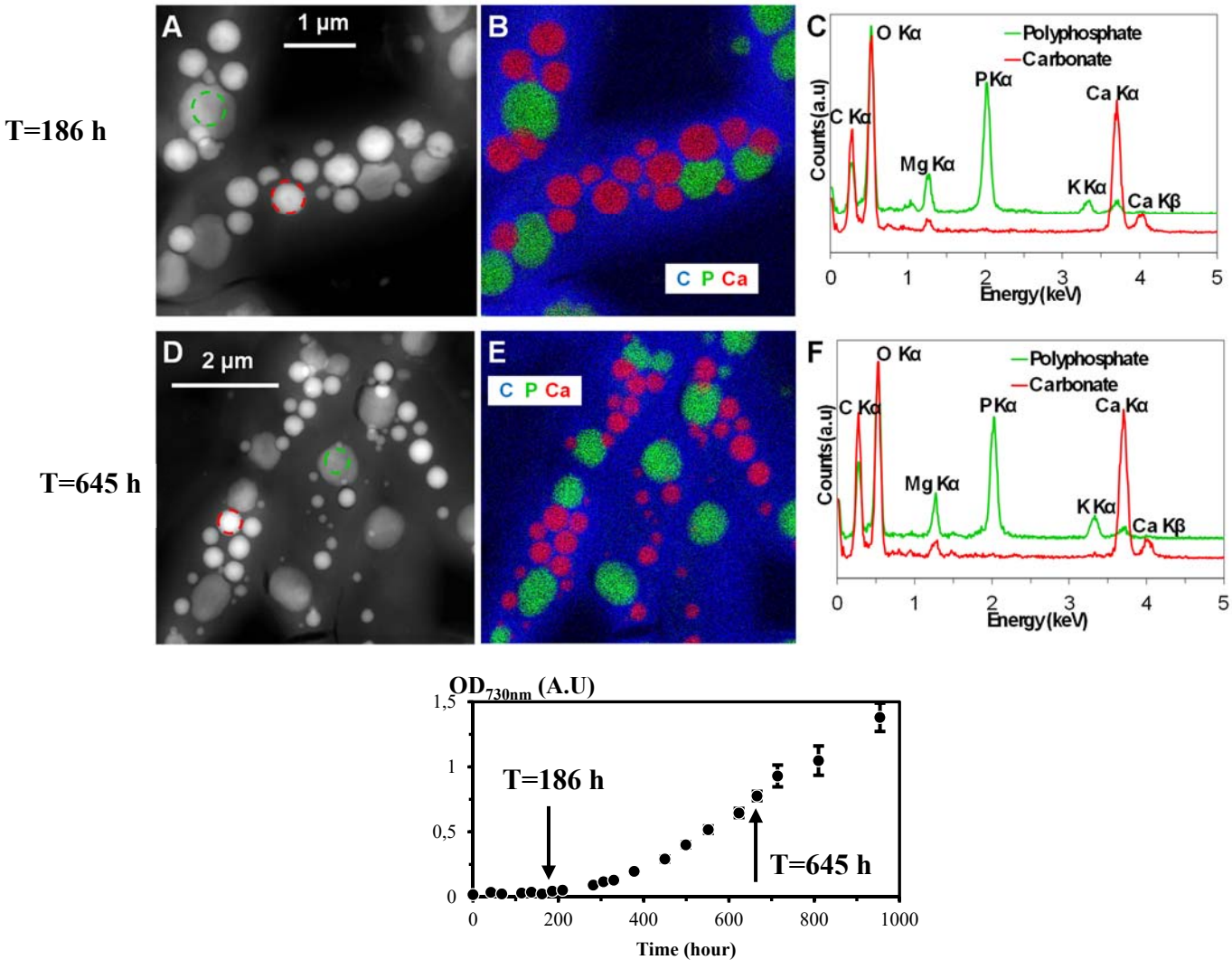
T=186 h
T=645 h
A
1 µm
B
C P Ca
C
O Kα
Polyphosphate
Carbonate
P Kα
Ca Kα
C Kα
Mg Kα
K Kα
Ca Kβ
Counts(a.u)
Energy(keV)
D
2 µm
E
C P Ca
F
O Kα
Polyphosphate
Carbonate
C Kα
P Kα
Ca Kα
Mg Kα
K Kα
Ca Kβ
Counts(a.u)
Energy(keV)
OD730nm (A.U)
T=186 h
T=645 h
Time (hour)

Figure 5

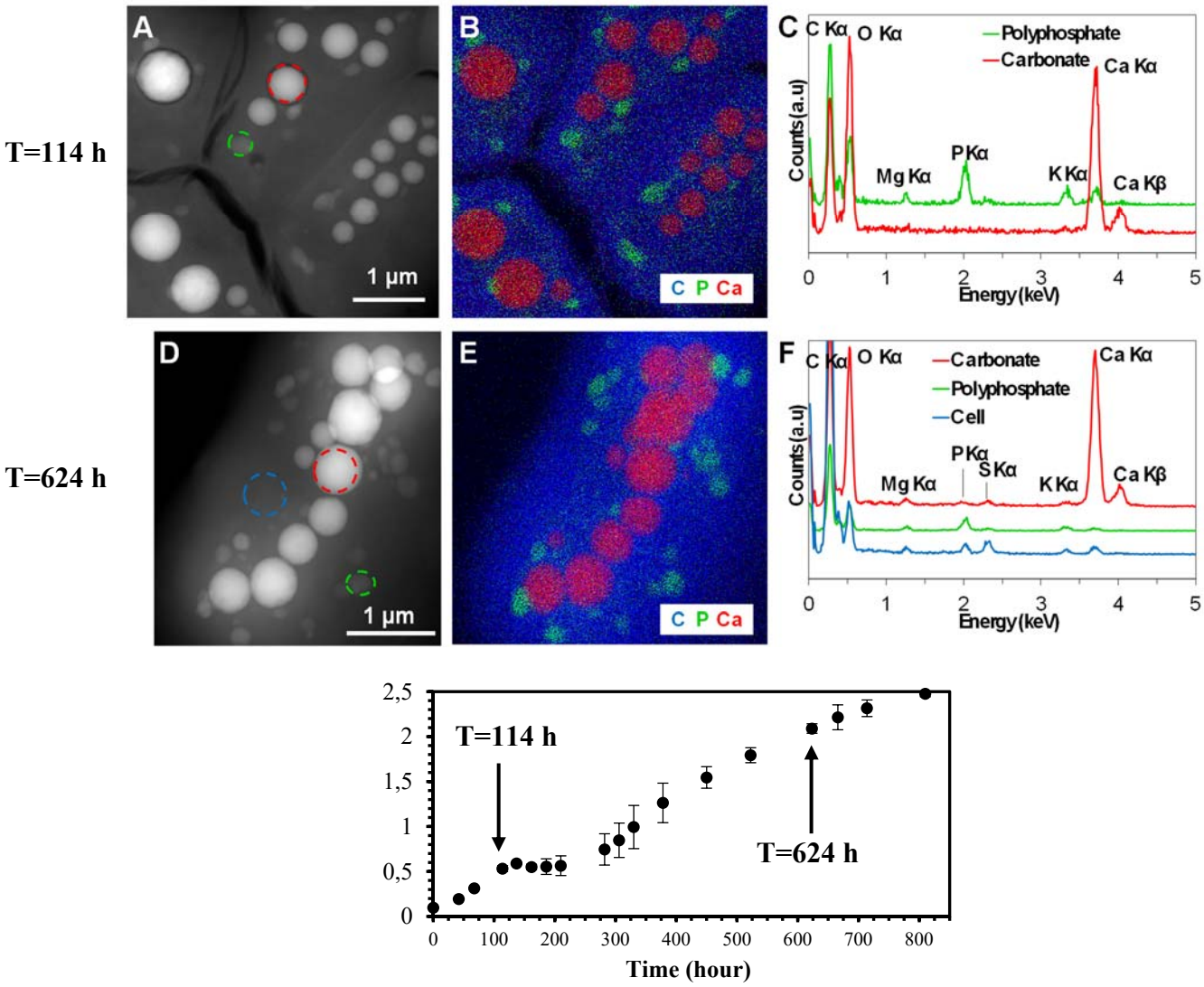
T=114 h
T=624 h
A
B
C
D
E
F
1 µm
C P Ca
C Kα
O Kα
Polyphosphate
Carbonate
Ca Kα
Mg Kα
P Kα
K Kα
Ca Kβ
Counts (a.u)
Energy (keV)
Cell
S Kα
T=114 h
T=624 h
Time (hour)

Figure 6

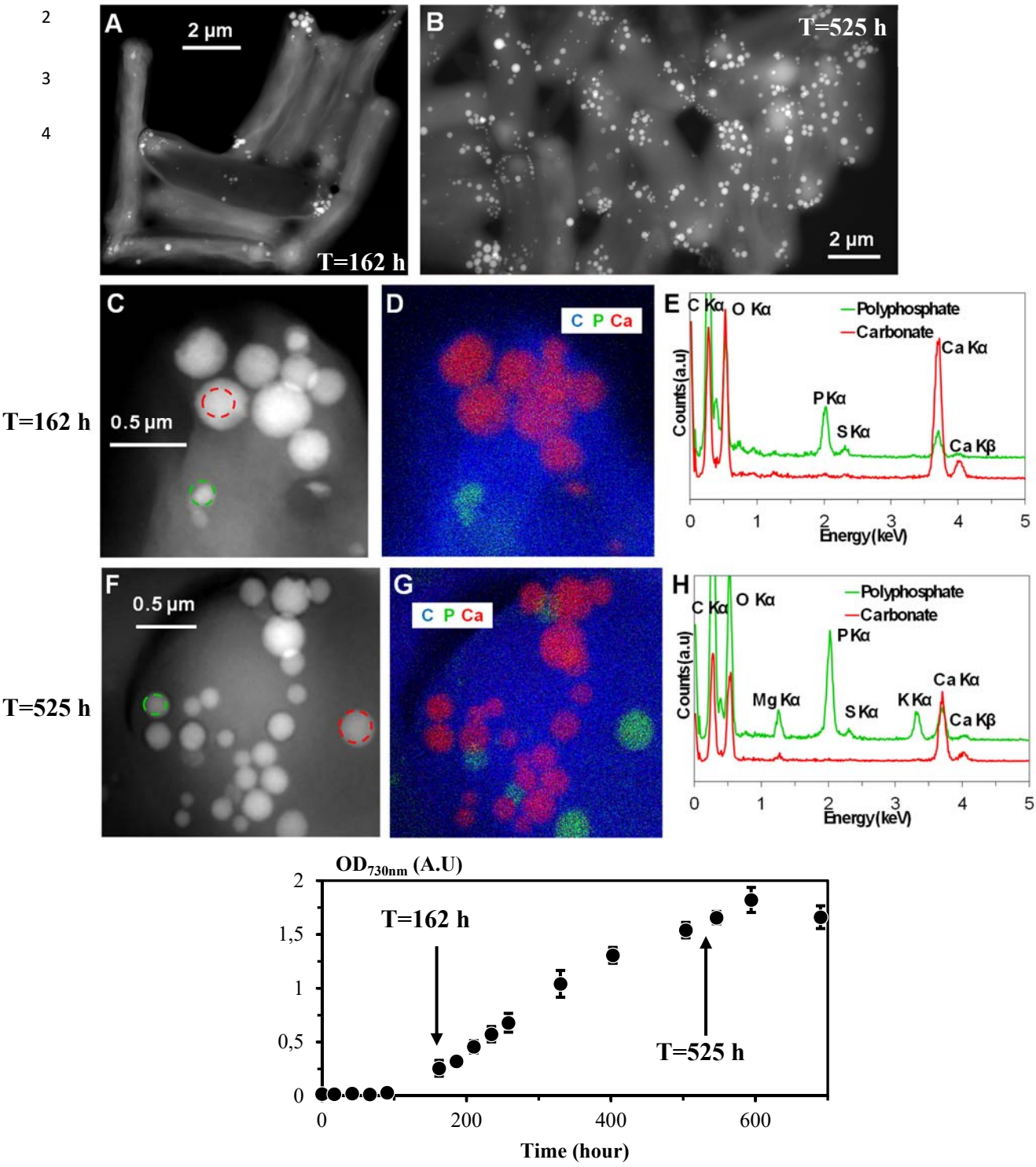
A
2 µm
T=162 h
B
T=525 h
2 µm
T=162 h
C
0.5 µm
D
C P Ca
E
C Kα
O Kα
Polyphosphate
Carbonate
Ca Kα
P Kα
S Kα
Ca Kβ
Counts(a.u)
Energy(keV)
T=525 h
F
0.5 µm
G
C P Ca
H
C Kα
O Kα
Polyphosphate
Carbonate
P Kα
Mg Kα
S Kα
K Kα
Ca Kα
Ca Kβ
Counts(a.u)
Energy(keV)
OD730nm (A.U)
T=162 h
T=525 h
Time (hour)

Figure 7

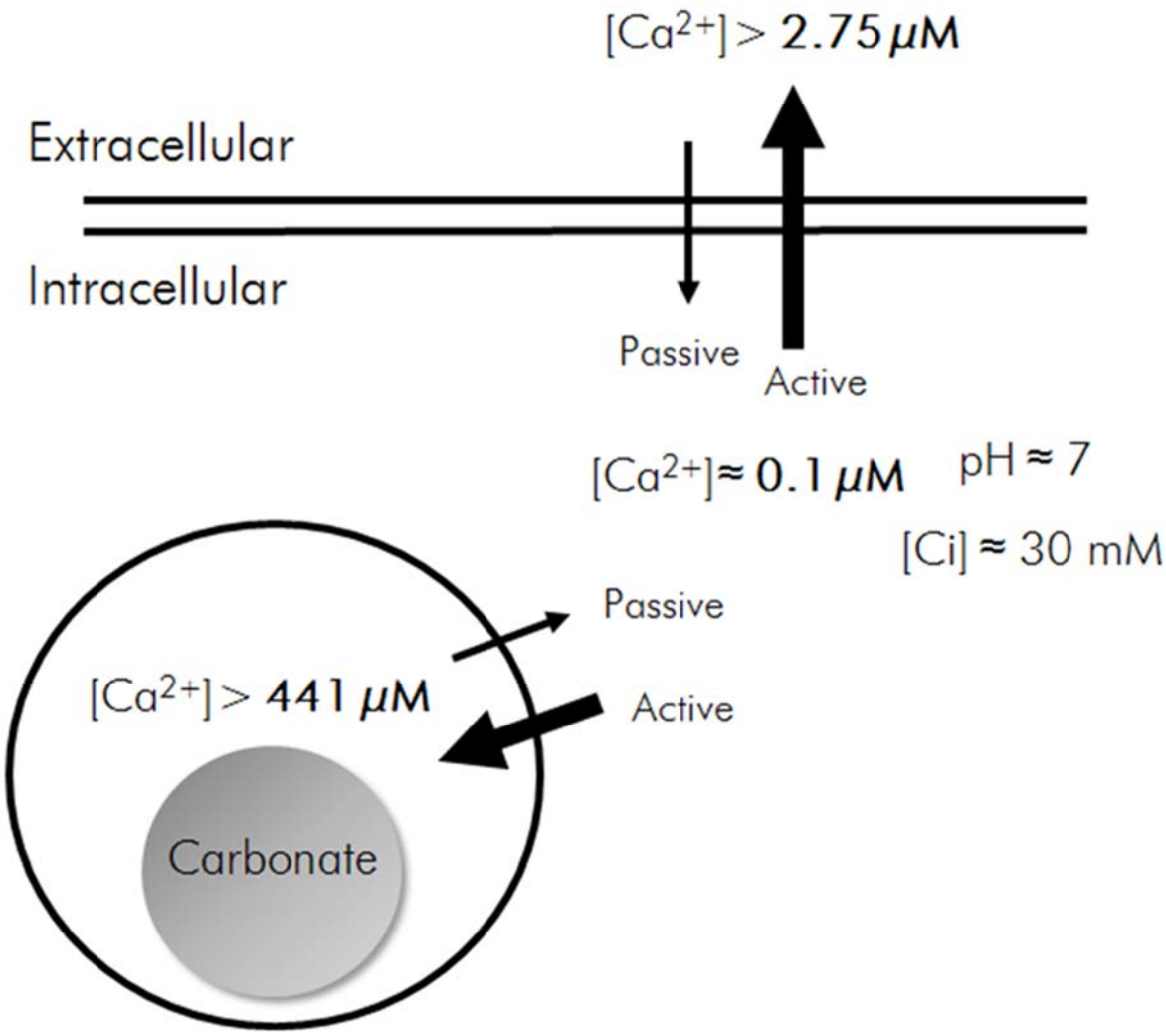
[Ca2+] > 2.75 μM
Extracellular
Intracellular
Passive
Active
[Ca2+] ≈ 0.1 μM
pH ≈ 7
[Ci] ≈ 30 mM
Passive
[Ca2+] > 441 μM
Active
Carbonate

Supplementary material includes 6 figures and 10 tables

Figure S1

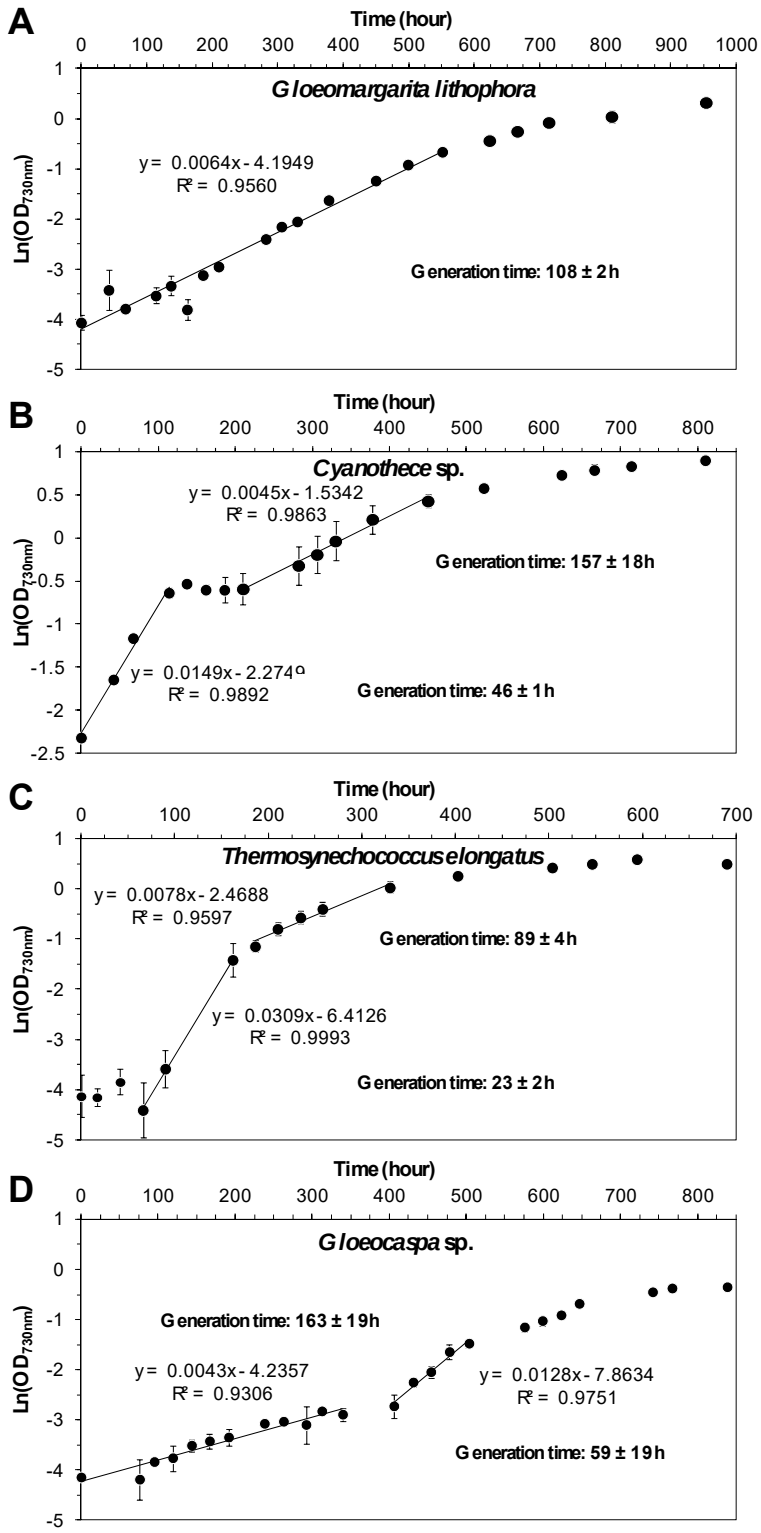

Figure S1: Growth of cultures of *Gloeomargarita lithophora* (A), *Cyanothece* sp. (B), *Thermosynechococcus elongatus* (C) and *Gloeocapsa* sp. (D) inoculated in BG-11.Several phases are discriminated in these graphs, marked by different generation times, i.e., slopes. Error bars were calculated based on variations in triplicates.

Figure S2

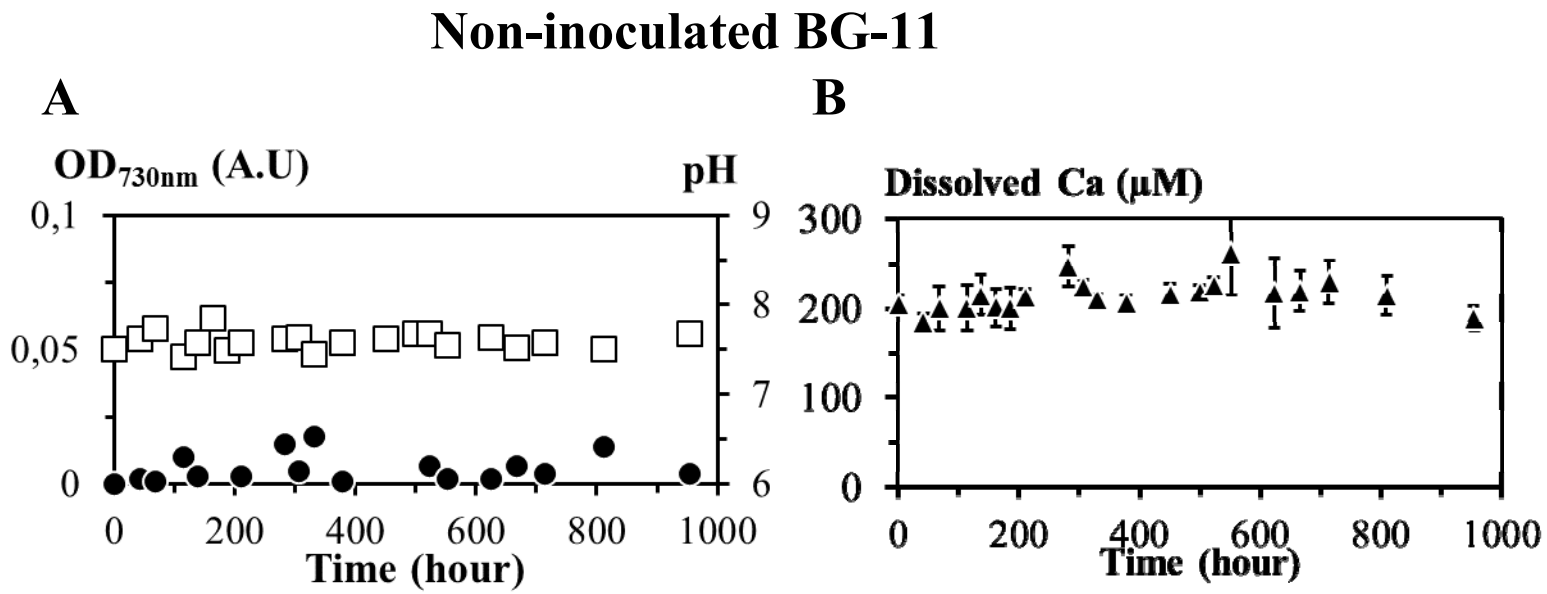

Figure S2: Time evolution of pH (open squares) and OD (closed circles) in (A) and dissolved Ca (closed triangles) in (B) in non-inoculated sterile BG-11 incubated at 30 °C under continuous light.

Figure S3

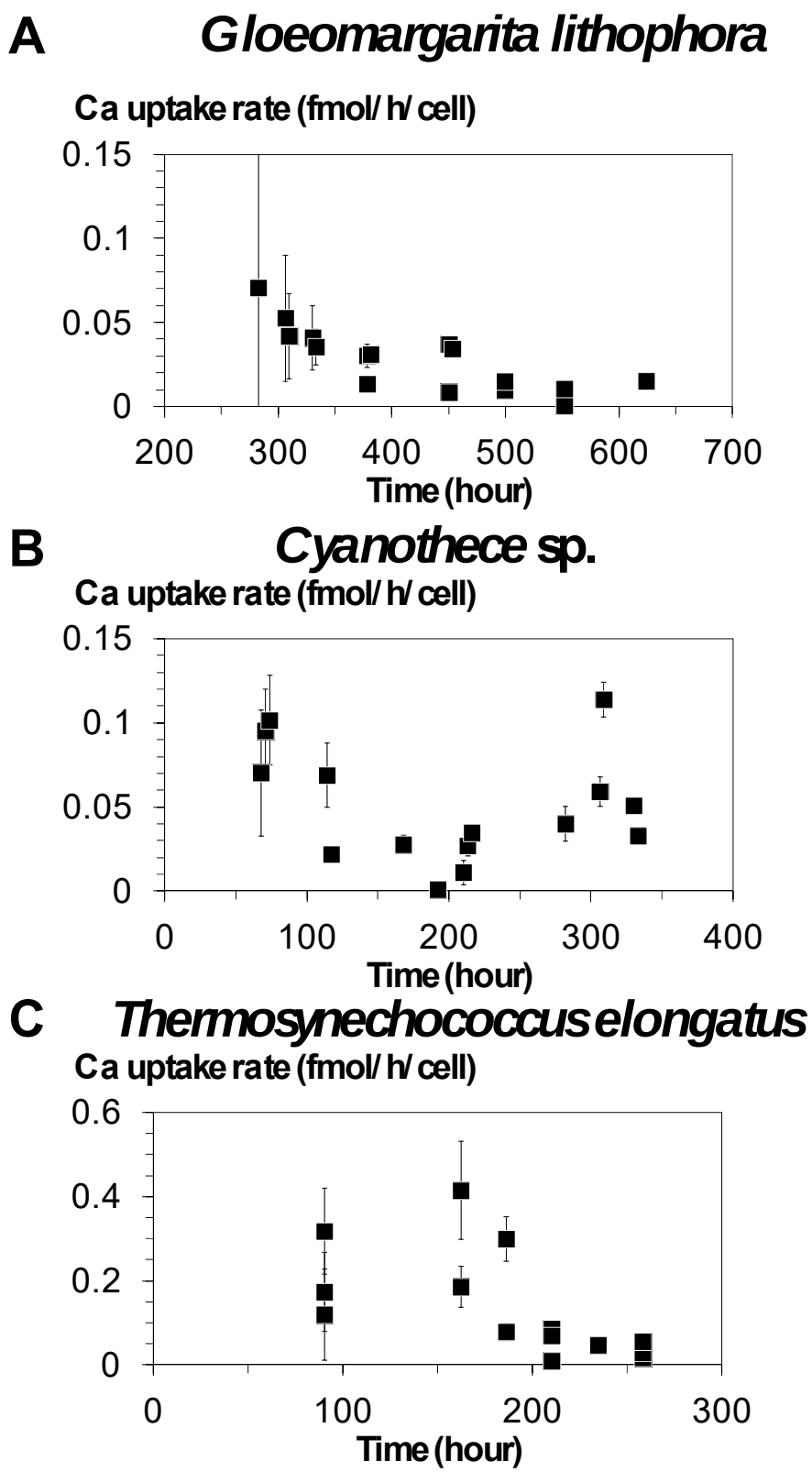

Figure S3: Uptake rate of Ca per cell versus time during the Ca uptake phase in cultures of *Gloeomargarita lithophora* (A), *Cyanothece* sp. (B) and *Thermosynechococcus elongatus* (C). Error bars were calculated based on instrumental precision. Values for the different replicates are reported in the graphs.

Figure S4

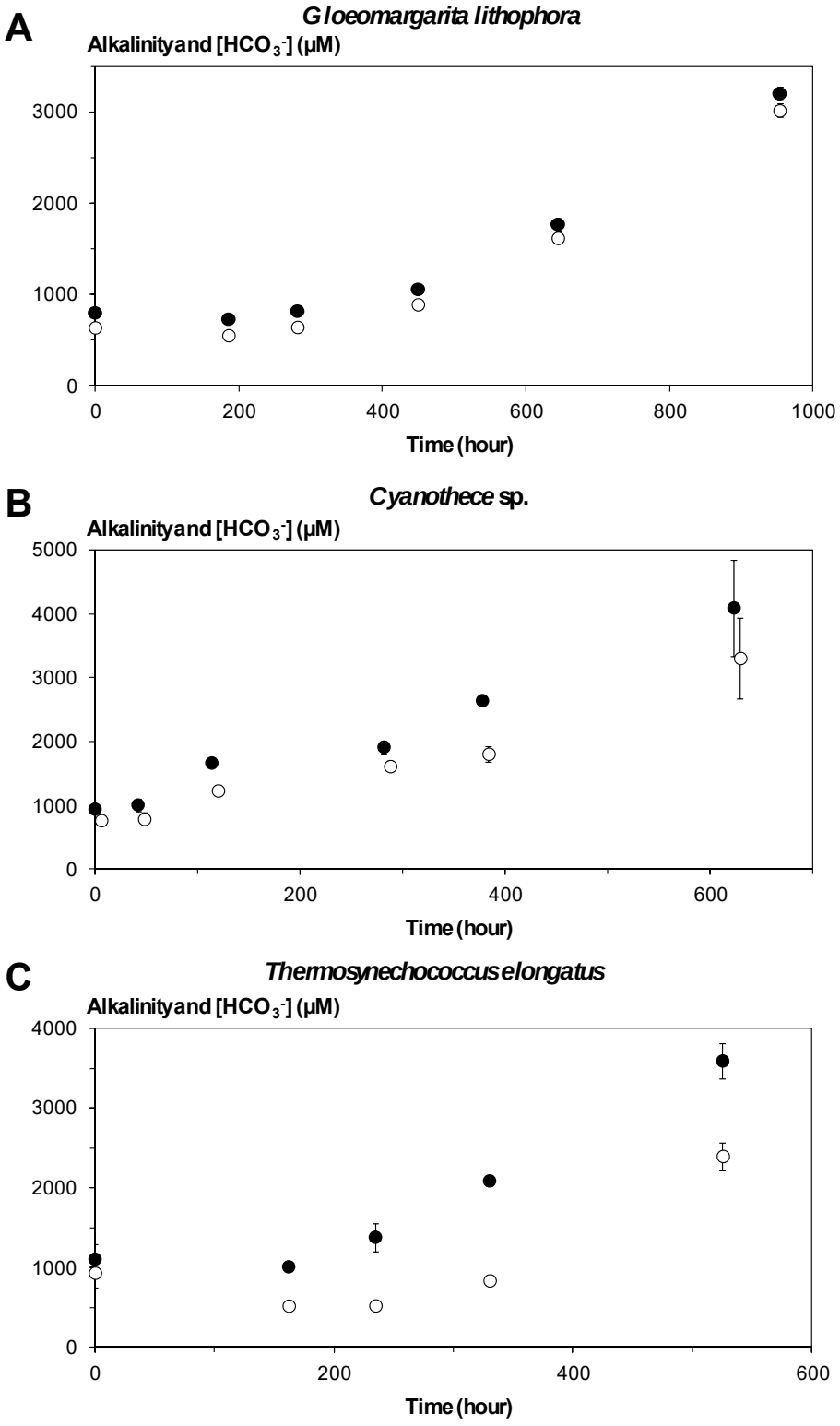

Figure S4: Time evolution of alkalinity (filled circles) and HCO_3^- (open circles) in extracellular solutions of *Gloeomargarita lithophora* (A), *Cyanothece* sp. (B) and *Thermosynechococcus elongatus* (C) cultures. Error bars were calculated based on variations in triplicates.

Figure S5

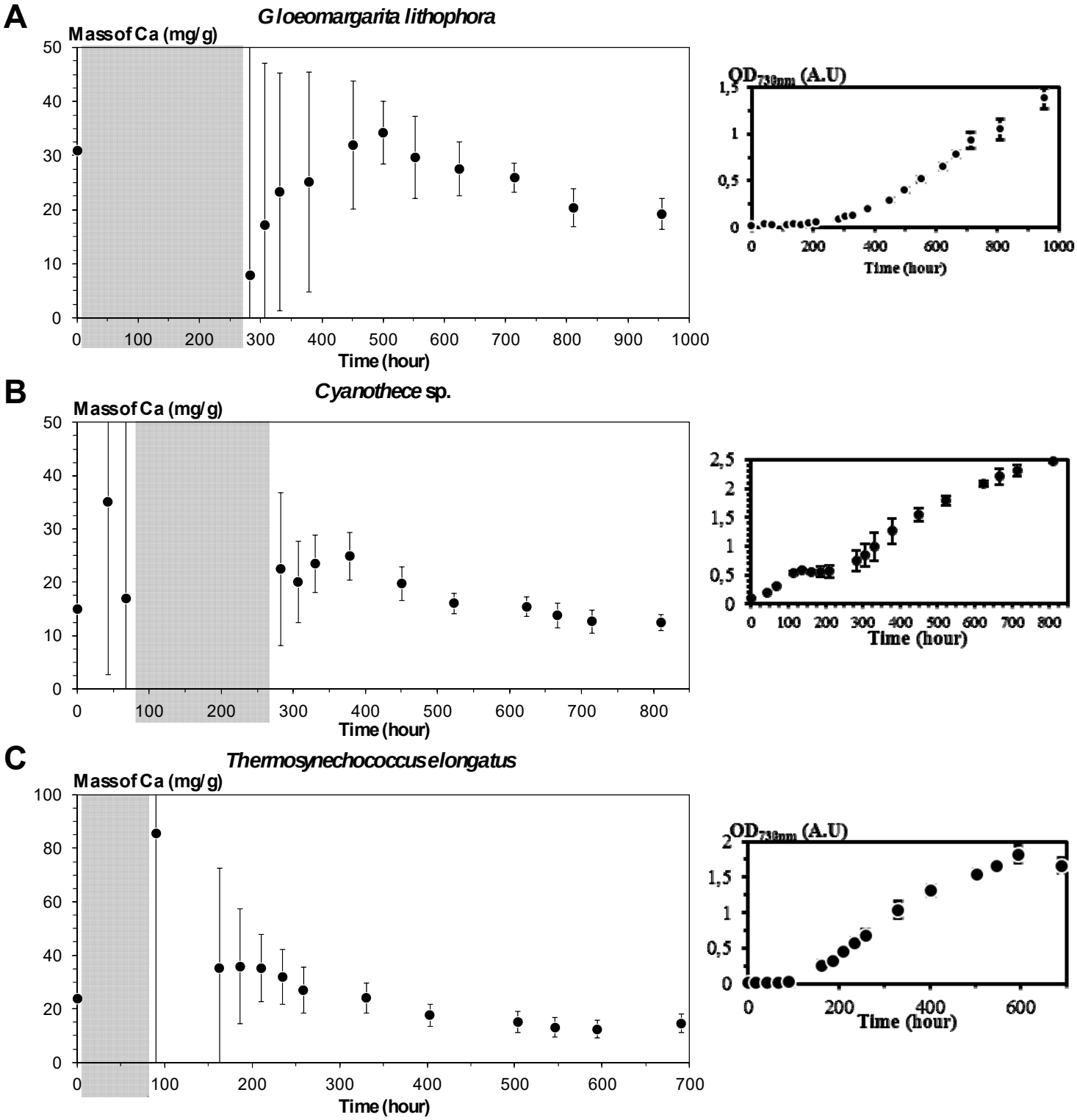

Fig. S5. Time evolution of the cellular mass proportion of Ca in cultures of *Gloeomargarita lithophora* (A), *Cyanothece* sp. (B) and *Thermosynechococcus elongatus* (C). The mass proportion of Ca was not calculated when no significant culture growth was observed. Standard deviations were calculated based on variations in triplicates and the precision of calcium concentration measurements. The grey areas correspond to lag phases and the transient phase with no growth for *Cyanothece sp.* culture. The same growth curves as in figure 1 are shown on the right.

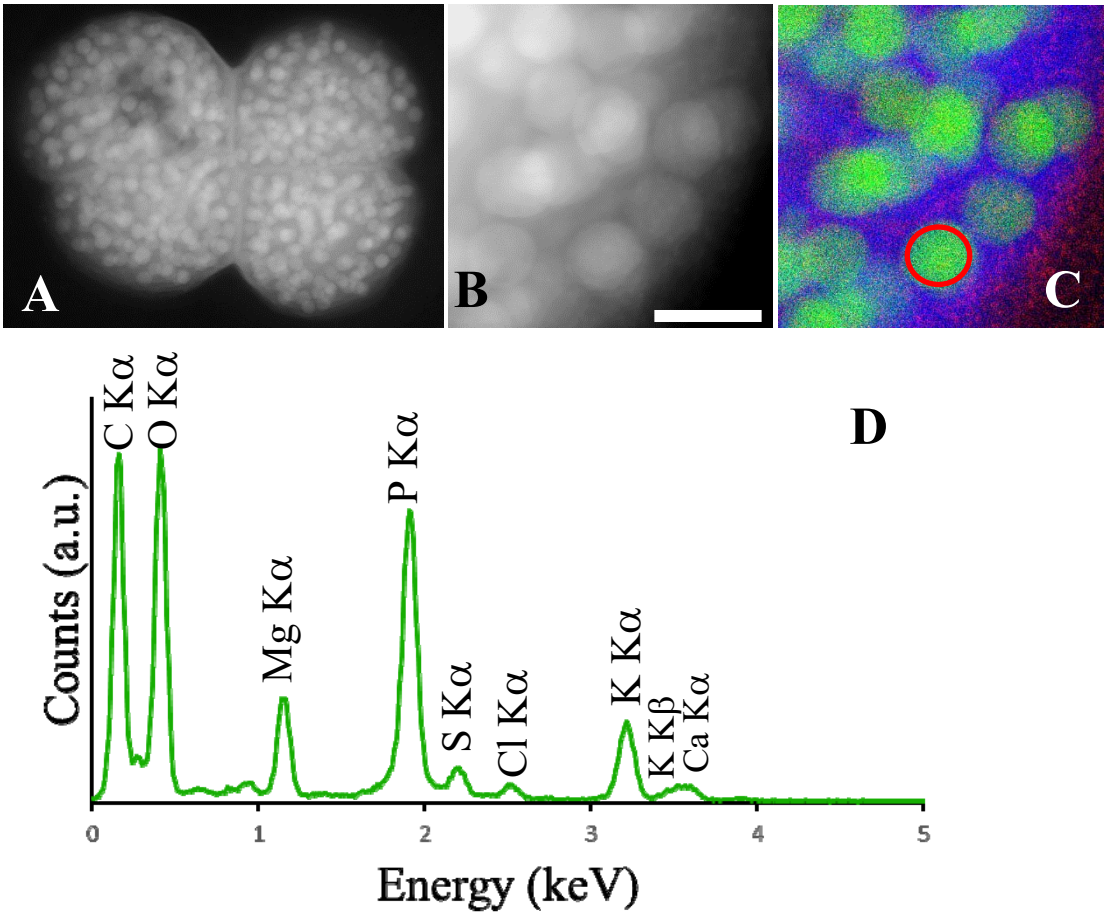

Figure S6: STEM-EDXS analyses of *Gloeocapsa sp.* cells. (A and B) STEM-HAADF images showing polyphosphate granules. (C) Corresponding EDXS maps of carbon (blue), phosphorus (green) and calcium (red). (D) EDXS spectrum of a P granule shown in C.

Table S1: Ca uptake rates, Ca affinities and cellular mass of Ca in cyanobacteria forming intracellular Ca-carbonates

Features	*Gloeomargarita lithophora*	*Cyanothece* sp.	*Thermosynechococcus elongatus*
Temperature (°C)	30	30	45
Final dissolved Ca (µM)	2.75 ± 0.54	5.9 ± 1.3	12.8 ± 3.6
Range of Ca uptake rate (fmol/cell/h)	0.01 - 0.07	0.001 - 0.11	0.01 - 0.42
Maximum measured cellular Ca mass ratio (mg/g of dry matter)	40	45	185

Time (h)		0	186	282	450	645	954
K	*repl. 1*	439	432	462	434	392	370
	repl. 2	395	437	445	426	402	380
	repl. 3	458	441	441	422	424	372
Mg	*repl. 1*	323	293	288	263	193	106
	repl. 2	287	292	284	260	199	105
	repl. 3	317	293	278	269	182	101
Na	*repl. 1*	18827	19788	19587	19018	19362	19165
	repl. 2	16813	19445	19519	18974	19819	19437
	repl. 3	18493	19652	19610	19706	19713	19261
N (NH_4^+ and NH_3)	*repl. 1*	20	14	23	15	23	36
	repl. 2	17	15	13	13	14	37
	repl. 3	26	10	23	20	20	33
N (NO_2^-)	*repl. 1*	4	14	15	31	157	838
	repl. 2	4	12	16	37	134	845
	repl. 3	4	13	16	34	199	988
N (NO_3^-)	*repl. 1*	20181	19955	19895	23132	22926	20902
	repl. 2	20522	18887	19707	23492	23325	20603
	repl. 3	20486	19813	19846	23685	23037	20272
Cl	*repl. 1*	507	529	533	542	515	523
	repl. 2	507	546	533	588	513	536
	repl. 3	508	531	537	543	513	518
S	*repl. 1*	377	380	384	374	318	262
	repl. 2	378	394	382	403	320	262
	repl. 3	379	383	384	375	313	256

Table S2: Chemical analyses of K, Mg, Na, S, Cl and N species as a function of time in *Gloeomargarita lithophora* cultures. Measurements were performed on triplicate cultures (3 lines per element). Concentrations are in μmol/L.

Table S3

Time (h)		0	42	114	186	282	378	623
K	*repl. 1*	438	451	452	-	445	420	412
	repl. 2	466	457	453	-	446	373	444
	repl. 3	449	464	441	425	424	-	421
Mg	*repl. 1*	314	295	281	-	279	258	234
	repl. 2	322	292	285	-	281	234	238
	repl. 3	320	290	282	281	267	-	238
Na	*repl. 1*	18675	19453	19436	-	19527	19469	19754
	repl. 2	18875	19683	19623	-	19762	17700	19984
	repl. 3	18833	19585	19538	19841	20076	-	19886
N (NH_4^+ and NH_3)	*repl. 1*	27	10	14	-	15	12	16
	repl. 2	31	10	16	-	23	10	20
	repl. 3	24	-	21	7	15	-	24
N (NO_2^-)	*repl. 1*	13	20	29	-	58	78	361
	repl. 2	16	21	36	-	65	88	354
	repl. 3	13	-	29	50	61	-	279
N(NO_3^-)	*repl. 1*	19685	19749	19194	-	18830	17570	19032
	repl. 2	19800	19801	19141	-	18905	17520	19033
	repl. 3	19805	-	19128	19146	17955	-	19344
Cl	*repl. 1*	512	519	527	-	535	542	527
	repl. 2	524	526	533	-	541	579	535
	repl. 3	515	525	537	533	540	-	534
S	*repl. 1*	375	369	356	-	333	290	208
	repl. 2	382	368	355	-	331	307	197
	repl. 3	375	371	358	337	310	-	190

Table S3: Chemical analyses of K, Mg, Na, S, Cl and N species as a function of time in *Cyanothece* sp. cultures. Measurements were performed on triplicate cultures. Concentrations are in µmol/L.

Table S4

Time (h)		0	162	234	330	525
K	*repl. 1*	454	463	-	436	424
	repl. 2	458	474	369	432	427
	repl. 3	464	455	430	426	428
Mg	*repl. 1*	297	269	-	164	109
	repl. 2	298	265	225	232	167
	repl. 3	305	281	266	250	195
Na	*repl. 1*	19625	20495	-	20553	19934
	repl. 2	19961	20527	16338	20226	19864
	repl. 3	19777	19673	18712	19946	19028
N (NH_4^+ and NH_3)	*repl. 1*	50	35	-	33	45
	repl. 2	48	33	30	34	33
	repl. 3	49	33	35	38	35
N (NO_2^-)	*repl. 1*	3	31	-	62	105
	repl. 2	3	32	47	69	143
	repl. 3	3	20	37	59	114
N(NO_3^-)	*repl. 1*	20052	19794	-	21996	20699
	repl. 2	19590	19460	18872	21706	20906
	repl. 3	20466	19423	18814	21683	20156
Cl	*repl. 1*	523	542	560	562	541
	repl. 2	520	542	564	550	527
	repl. 3	522	529	535	550	515
S	*repl. 1*	434	416	399	346	246
	repl. 2	432	414	402	348	255
	repl. 3	439	418	397	364	258

Table S4: Chemical analyses of K, Mg, Na, S, Cl and N species as a function of time in *Thermosynechococcus elongatus* cultures. Measurements were performed on triplicate cultures. Concentrations are in µmol/L.

Table S5

Time (h)	0	186	282	450	645	954
	-2.906	-1.946	-2.466	-1.387	-2.095	-2.325
ACC	-2.906	-1.946	-2.466	-1.387	-2.095	-2.325
	-2.95	-2.444	-1.99	-1.291	-2.185	-2.492
	-2.223	-1.262	-1.783	-0.704	-1.411	-1.642
Aragonite	-2.223	-1.262	-1.783	-0.704	-1.411	-1.642
	-2.266	-1.76	-1.306	-0.608	-1.501	-1.809
	-2.082	-1.122	-1.642	-0.564	-1.271	-1.502
Calcite	-2.082	-1.122	-1.642	-0.564	-1.271	-1.502
	-2.126	-1.62	-1.166	-0.468	-1.361	-1.668
	-2.636	-1.675	-2.196	-1.117	-1.825	-2.055
Vaterite	-2.636	-1.675	-2.196	-1.117	-1.825	-2.055
	-2.679	-2.174	-1.719	-1.021	-1.914	-2.222
	-4.341	-2.417	-3.431	-0.959	-1.036	-1.74
Dolomite	-4.341	-2.417	-3.431	-0.959	-1.036	-1.74
	-4.44	-3.415	-2.468	-0.847	-1.059	-2.02
	4.901	6.835	5.631	6.304	-2.02	-6.793
Hydroxyapatite	4.901	6.835	5.631	6.304	-2.02	-6.793
	4.927	5.86	6.571	6.885	-6.836	-7.302
	-4.173	-3.203	-3.833	-3.744	-9.057	-12.162
$Ca_3(PO_4)_2$ (am1)	-4.173	-3.203	-3.833	-3.744	-9.057	-12.162
	-4.141	-3.687	-3.364	-3.388	-12.238	-12.446
	-1.443	-0.473	-1.103	-1.014	-6.328	-9.432
$Ca_3(PO_4)_2$ (am2)	-1.443	-0.473	-1.103	-1.014	-6.328	-9.432
	-1.411	-0.957	-0.635	-0.658	-9.508	-9.716
	-1.18	-0.211	-0.84	-0.751	-6.065	-9.17
$Ca_3(PO_4)_2$ (beta)	-1.18	-0.211	-0.84	-0.751	-6.065	-9.17
	-1.149	-0.695	-0.372	-0.396	-9.245	-9.454
	-2.148	-1.174	-1.857	-2.263	-9.88	-14.422
$Ca_4H(PO_4)_3{:}3H_2O$(s)	-2.148	-1.174	-1.857	-2.263	-9.88	-14.422
	-2.078	-1.65	-1.393	-1.778	-14.606	-14.765
	-3.405	-2.445	-2.965	-1.887	-2.594	-2.825
$CaCO_3xH_2O$(s)	-3.405	-2.445	-2.965	-1.887	-2.594	-2.825
	-3.449	-2.943	-2.489	-1.791	-2.684	-2.991
	-1.271	-1.267	-1.321	-1.816	-4.119	-5.556
$CaHPO_4$(s)	-1.271	-1.267	-1.321	-1.816	-4.119	-5.556
	-1.234	-1.259	-1.325	-1.686	-5.664	-5.615
	-1.528	-1.524	-1.578	-2.073	-4.376	-5.813
$CaHPO_4{:}2H_2O$(s)	-1.528	-1.524	-1.578	-2.073	-4.376	-5.813
	-1.49	-1.516	-1.582	-1.943	-5.921	-5.872

Table S5: Saturation indices as a function of time of the extracellular solution of *Gloeomargarita lithophora* cultures with diverse carbonate and Ca-phosphate phases. Calculations were performed for triplicate cultures (3 lines per mineral phase).

Table S6

Time (h)	0	42	114	186	282	378	623
	-2.698	-1.483	-0.279		-0.627	-0.936	-1.31
ACC	-2.604	-1.303	0.027		-0.61	-1.218	-1.122
	-2.43		0.202	-1.336	-1.49		-1.133
	-2.015	-0.799	0.404		0.057	-0.252	-0.627
Aragonite	-1.92	-0.62	0.711		0.074	-0.534	-0.439
	-1.746		0.885	-0.653	-0.806		-0.449
	-1.874	-0.659	0.545		0.197	-0.112	-0.487
Calcite	-1.78	-0.48	0.851		0.214	-0.394	-0.298
	-1.606		1.026	-0.512	-0.666		-0.309
	-2.428	-1.212	-0.009		-0.356	-0.665	-1.04
Vaterite	-2.333	-1.033	0.297		-0.339	-0.947	-0.852
	-2.159		0.472	-1.066	-1.219		-0.862
	-3.913	-1.437	1.269		0.459	1.255	0.527
Dolomite	-3.728	-1.066	2.042		0.551	0.834	0.737
	-3.378		2.487	-0.79	0.079		0.699
	5.429	7.739	8.852		8.595	1.916	1.374
Hydroxyapatite	5.68	8.042	8.397		8.411	1.242	2.105
	6.049		7.218	6.711	2.455		2.401
	-3.89	-2.755	-2.414		-2.47	-6.819	-7.056
$Ca_3(PO_4)_2$ (am1)	-3.754	-2.613	-2.82		-2.598	-7.175	-6.631
	-3.566		-3.664	-3.49	-6.275		-6.431
	-1.16	-0.025	0.316		0.26	-4.09	-4.326
$Ca_3(PO_4)_2$ (am2)	-1.024	0.117	-0.09		0.132	-4.445	-3.901
	-0.837		-0.934	-0.76	-3.545		-3.701
	-0.897	0.237	0.578		0.523	-3.827	-4.064
$Ca_3(PO_4)_2$ (beta)	-0.762	0.379	0.173		0.394	-4.182	-3.639
	-0.574		-0.671	-0.497	-3.283		-3.438
	-1.827	-0.733	-0.823		-0.733	-7.103	-7.27
$Ca_4H(PO_4)_3{:}3H_2O$(s)	-1.671	-0.609	-1.584		-0.933	-7.495	-6.727
	-1.476		-2.938	-1.908	-6.01		-6.421
	-3.197	-1.982	-0.778		-1.126	-1.435	-1.81
$CaCO_3xH_2O$(s)	-3.103	-1.802	-0.472		-1.109	-1.717	-1.621
	-2.929		-0.297	-1.835	-1.989		-1.632
	-1.234	-1.274	-1.705		-1.559	-3.58	-3.511
$CaHPO_4$(s)	-1.213	-1.293	-2.061		-1.632	-3.616	-3.392
	-1.206		-2.571	-1.715	-3.031		-3.287
	-1.491	-1.531	-1.962		-1.816	-3.837	-3.767
$CaHPO_4{:}2H_2O$(s)	-1.47	-1.55	-2.318		-1.889	-3.873	-3.649
	-1.463		-2.828	-1.971	-3.288		-3.544

Table S6: Saturation indices as a function of time of the extracellular solution of *Cyanothece* sp. cultures with diverse carbonate and Ca-phosphate phases. Calculations were performed for triplicate cultures.

Table S7

Time (h)	0	162	234	330	525
ACC	-2.663	0.393		-0.819	-0.722
	-2.624	0.406	0.126	-0.562	-0.617
	-2.73	0.34	0.268	-0.375	-0.577
Aragonite	-2.006	1.05		-0.162	-0.065
	-1.967	1.063	0.783	0.096	0.04
	-2.073	0.997	0.925	0.282	0.08
Calcite	-1.876	1.18		-0.031	0.065
	-1.837	1.193	0.913	0.226	0.171
	-1.942	1.128	1.055	0.412	0.21
Vaterite	-2.392	0.663		-0.548	-0.452
	-2.354	0.676	0.396	-0.291	-0.346
	-2.459	0.611	0.539	-0.105	-0.306
Dolomite	-3.806	2.823		1.539	1.224
	-3.745	2.905	2.659	1.914	1.549
	-3.941	2.409	2.736	2.132	1.581
Hydroxyapatite	5.549	7.261		-1.103	2.721
	5.675	6.02	2.491	0.884	3.049
	5.423	10.149	5.989	1.742	3.914
$Ca_3(PO_4)_2$ (am1)	-3.014	-2.891		-8.064	-5.546
	-2.943	-3.723	-5.983	-6.825	-5.363
	-3.076	-0.949	-3.698	-6.314	-4.799
$Ca_3(PO_4)_2$ (am2)	-0.341	-0.219		-5.391	-2.873
	-0.27	-1.05	-3.31	-4.152	-2.69
	-0.403	1.724	-1.025	-3.642	-2.126
$Ca_3(PO_4)_2$ (beta)	-1.224	-1.101		-6.274	-3.756
	-1.153	-1.933	-4.193	-5.035	-3.573
	-1.286	0.841	-1.908	-4.524	-3.009
$Ca_4H(PO_4)_3{:}3H_2O$ (s)	-0.757	-2.102		-9.254	-5.526
	-0.671	-3.355	-6.605	-7.524	-5.304
	-0.817	0.839	-3.249	-6.852	-4.479
$CaCO_3xH_2O$ (s)	-3.126	-0.07		-1.282	-1.185
	-3.087	-0.057	-0.337	-1.024	-1.08
	-3.193	-0.123	-0.195	-0.838	-1.04
$CaHPO_4$ (s)	-1.381	-2.848		-4.828	-3.618
	-1.365	-3.27	-4.26	-4.337	-3.579
	-1.379	-1.85	-3.188	-4.175	-3.317
$CaHPO_4{:}2H_2O$ (s)	-1.573	-3.04		-5.02	-3.809
	-1.557	-3.462	-4.452	-4.529	-3.771
	-1.571	-2.042	-3.38	-4.367	-3.509

Table S7: Saturation indices as a function of time of the extracellular solution of *Thermosynechococcus elongatus* cultures with respect to diverse carbonate and Ca-phosphate phases. Calculations were performed for triplicate cultures.

Gloeomargarita lithophora

Time (h)	STEM (HAADF) Number of analyzed cells (empty cells)	Number of analyzed carbonates granules	$CaCO_3$ granules per cell	$CaCO_3$ granules diameter (nm)	Volume of $CaCO_3$ per cell (μm^3)
0	31 (2)	219	7.6 ± 3.0	218 ± 82	0.059 ± 0.033
186	54 (12)	369	8.8 ± 5.9	221 ± 89	0.076 ± 0.071
282	116 (23)	765	8.2 ± 4.3	201 ± 86	0.055 ± 0.046
450	83 (16)	520	7.8 ± 4.7	211 ± 80	0.056 ± 0.040
645	86 (8)	508	6.5 ± 2.8	204 ± 82	0.045 ± 0.037
954	-	411	-	197 ± 68	-

Time (h)	EDXS **Mg ratio (Mg/Mg+Ca)**	STEM-EDXS **Mass of Ca in $CaCO_3$ granules** (mg/g of dry matter)	ICP-AES **Total Ca in cells** (mg/g of dry matter)	**Part of cellular Ca in $CaCO_3$ granules** (%)
0	10.4 ± 1.9	9.6 ± 5.6	31	31 ± 18
186	9.8 ± 2.0	12 ± 12	45 ± 29	27 ± 32
282	10.1 ± 2.1	9.0 ± 7.7	45 ± 16	20 ± 19
450	11.6 ± 2.6	9.0 ± 6.7	46.7 ± 2.5	19 ± 14
645	14.8 ± 5.1	7.0 ± 6.2	33.3 ± 0.7	21 ± 19
954	39 ± 18	-	17.3 ± 2.1	-

Table S8. Time evolution of intracellular carbonates in *Gloeomargarita lithophora*. The total number of analyzed cells (with and without granules) ~~The number of cells containing carbonate granules~~ is indicated. Empty cells (i.e., with no detected carbonate granule) are indicated in brackets. Numbers of analyzed carbonate granules, number of carbonate granule per cell, their diameters and their volume were estimated from on STEM-HAADF measurements. The Mg/(Mg+Ca) ratios in $CaCO_3$ granules were determined by EDXS analyses. The mass of Ca in $CaCO_3$ granules was determined by multiplying the volume of $CaCO_3$ per cell by the density of ACC (2.18 from Fernandez-Martinez *et al.*, 2013) taking into account the mass proportion of Ca per $CaCO_3$ granule. The mass of total Ca in cells was the difference between the initial concentration of Ca in BG-11 minus the concentration of dissolved Ca at a given time, divided by the number of cells at the same time. The percent of Ca in $CaCO_3$ granules was the mass of Ca in $CaCO_3$ granules by the total mass of Ca in cells.

Cyanothece sp.

Time (h)	STEM (HAADF) Number of analyzed: cells (empty cells)	carbonates granules	$CaCO_3$ granules per cell	$CaCO_3$ granules diameter (nm)	Volume of $CaCO_3$ per cell (μm^3)
0	16 (4)	82	6.8 ± 3.4	277 ± 126	0.128 ± 0.092
42	47 (7)	145	3.6 ± 2.1	279 ± 139	0.075 ± 0.055
114	132 (10)	555	4.5 ± 2.0	317 ± 122	0.113 ± 0.070
282	85 (18)	316	4.7 ± 3.6	282 ± 109	0.083 ± 0.074
623	97 (35)	280	4.5 ± 2.9	300 ± 151	0.117 ± 0.125

Time (h)	EDXS Mg ratio (Mg/Mg+Ca)	STEM-EDXS Mass of Ca in $CaCO_3$ granules (mg/g of dry matter)	ICP-AES Total Ca in cells (mg/g of dry matter)	Part of cellular Ca in $CaCO_3$ granules (%)
0	4.0 ± 2.2	11 ± 11	15	76 ± 70
42	4.4 ± 2.2	6.7 ± 5.9	42.3 ± 4.9	16 ± 14
114	3.0 ± 1.7	10.2 ± 8.5	42.9 ± 1.5	24 ± 20
282	4.8 ± 2.2	7.4 ± 7.4	30.1* ± 1.2*	25* ± 25*
623	3.2 ± 0.9	11 ± 12	17.9* ± 0.1*	60* ± 66*

Table S9. Time evolution of intracellular carbonates in *Cyanothece* sp. * indicates that measurements were performed on two replicates only, while all other measurements were obtained from three replicates.

Thermosynechococcus elongatus

	STEM (HAADF)											
	Number of analyzed		**$CaCO_3$ granules per cell**			**$CaCO_3$ granules diameter**			**Volume of $CaCO_3$ per cell**		
Time (h)	cells (empty cells)	carbonate granules				(nm)			(μm^3)		
0	44 (6)	152	4.0	±	2.6	111	±	66	0.006	±	0.006
234	85 (3)	596	7.3	±	4.7	129	±	62	0.015	±	0.020
330	103 (2)	565	5.6	±	2.6	131	±	72	0.014	±	0.017
525	92 (19)	1656	22.7	±	9.6	172	±	64	0.087	±	0.045
	EDXS		STEM-EDXS			ICP-AES					
Time (h)	**Mg ratio (Mg/Mg+Ca)**		**Mass of Ca in $CaCO_3$ granules** (mg/g of dry matter)			**Total Ca in cells** (mg/g of dry matter)			**Part of cellular Ca in $CaCO_3$ granules** (%)		
0	4.1	± 1.5	0.4	±	0.4	24			1.5	±	1.5
234	3.7	± 1.2	0.8	±	1.1	35.6*	±	0.9*	2.3*	±	3.2*
330	3.7	± 1.8	0.8	±	1.0	25.6	±	2.6	3.1	±	4.1
525	7.6	± 2.4	4.7	±	2.8	16.4	±	0.6	29	±	17

Table S10. Time evolution of intracellular carbonates in *Thermosynechococcus elongatus*.
* indicates that measurements were performed on two replicates only, while all other measurements were obtained from three replicates.